

1 **Dissolved iron in the North Atlantic Ocean and Labrador**  
2 **Sea along the GEOVIDE section (GEOTRACES section**  
3 **GA01)**

4 Manon Tonnard<sup>1,2,3</sup>, H el ene Planquette<sup>1</sup>, Andrew R. Bowie<sup>2,3</sup>, Pier van der Merwe<sup>2</sup>,  
5 Morgane Gallinari<sup>1</sup>, Floriane Desprez de G esincourt<sup>1</sup>, Yoan Germain<sup>4</sup>, Arthur  
6 Gourain<sup>5</sup>, Marion Benetti<sup>6,7</sup>, Gilles Reverdin<sup>7</sup>, Paul Tr eguer<sup>1</sup>, Julia Boutorh<sup>1</sup>, Marie  
7 Cheize<sup>1</sup>, Fran ois Lacan<sup>8</sup>, Jan-Lukas Menzel Barraqueta<sup>9,10</sup>, Leonardo Pereira-  
8 Contreira<sup>11</sup>, Rachel Shelley<sup>1,12,13</sup>, Pascale Lherminier<sup>14</sup>, G eraldine Sarthou<sup>1</sup>

9 <sup>1</sup>Univ Brest, CNRS, IRD, Ifremer, LEMAR, F-29280 Plouzane, France

10 <sup>2</sup>Antarctic Climate and Ecosystems – Cooperative Research Centre, University of Tasmania, Hobart,  
11 TAS 7001, Australia

12 <sup>3</sup>Institute for Marine and Antarctic Studies, University of Tasmania, Hobart, TAS 7001, Australia

13 <sup>4</sup>Laboratoire Cycles G eochimiques et ressources – Ifremer, Plouzan e, 29280, France

14 <sup>5</sup>Ocean Sciences Department, School of Environmental Sciences, University of Liverpool, L69 3GP, UK

15 <sup>6</sup>Institute of Earth Sciences, University of Iceland, Reykjavik, Iceland

16 <sup>7</sup>LOCEAN, Sorbonne Universit es, UPMC/CNRS/IRD/MNHN, Paris, France

17 <sup>8</sup>LEGOS, Universit e de Toulouse - CNRS/IRD/CNES/UPS – Observatoire Midi-Pyr en ees, Toulouse,  
18 France

19 <sup>9</sup>GEOMAR Helmholtz-Zentrum f ur Ozeanforschung Kiel Wischhofstra e 1-3, Geb. 12 D-24148 Kiel,  
20 Germany

21 <sup>10</sup>Department of Earth Sciences, Stellenbosch University, Stellenbosch, 7600, South Africa

22 <sup>11</sup>Funda  o Universidade Federal do Rio Grande (FURG), R. Luis Lor ea, Rio Grande –RS, 96200-350,  
23 Brazil

24 <sup>12</sup>Dept. Earth, Ocean and Atmospheric Science, Florida State University, 117 N Woodward Ave,  
25 Tallahassee, Florida, 32301, USA

26 <sup>13</sup>School of Geography, Earth and Environmental Sciences, University of Plymouth, Drake Circus,  
27 Plymouth, PL4 8AA, UK

28 <sup>14</sup> Ifremer, Univ Brest, CNRS, IRD, Laboratoire d'Océanographie Physique et Spatiale (LOPS), IUEM,  
29 F-29280, Plouzané, France

30 *Correspondence to:* geraldine.sarthou@univ-brest.fr; helene.planquette@univ-brest.fr

31

32

33

34 **Abstract.**

35 Dissolved Fe (DFe) samples from the GEOVIDE voyage (GEOTRACES GA01, May-June 2014) in the  
36 North Atlantic Ocean were analysed using a SeaFAST-pico™ coupled to an Element XR SF-ICP-MS  
37 and provided interesting insights on the Fe sources in this area. Overall, DFe concentrations ranged  
38 from  $0.09 \pm 0.01 \text{ nmol L}^{-1}$  to  $7.8 \pm 0.5 \text{ nmol L}^{-1}$ . Elevated DFe concentrations were observed above the  
39 Iberian, Greenland and Newfoundland Margins likely due to riverine inputs from the Tagus River,  
40 meteoric water inputs and sedimentary inputs. Deep winter convection occurring the previous winter  
41 provided iron-to-nitrate ratios sufficient to sustain phytoplankton growth and lead to relatively elevated  
42 DFe concentrations within subsurface waters of the Irminger Sea. Increasing DFe concentrations along  
43 the flow path of the Labrador Sea Water were attributed to sedimentary inputs from the Newfoundland  
44 Margin. Bottom waters from the Irminger Sea displayed high DFe concentrations likely due to the  
45 dissolution of Fe-rich particles in the Denmark Strait Overflow Water and the Polar Intermediate Water.  
46 Finally, the nepheloid layers located in the different basins and at the Iberian Margin were found to act  
47 as either a source or a sink of DFe depending on the nature of particles with organic particles likely  
48 releasing DFe and Mn-particles scavenging DFe.

49

50 **1 Introduction**

51 The North Atlantic Ocean is known for its pronounced spring phytoplankton blooms (Henson et al., 2009;  
52 Longhurst, 2007). Phytoplankton blooms induce the capture of aqueous carbon dioxide through  
53 photosynthesis, and conversion into particulate organic carbon (POC). This POC is then exported into  
54 deeper waters through sinking and ocean currents. Via these processes, and in conjunction with the  
55 physical carbon pump, the North Atlantic Ocean is the largest oceanic sink of anthropogenic CO<sub>2</sub> (Pérez  
56 et al., 2013), despite covering only 15% of global ocean area (Humphreys et al., 2016; Sabine et al.,  
57 2004) and is therefore crucial for Earth's climate.

58 Indeed, phytoplankton must obtain, besides light and inorganic carbon, chemical forms of essential  
59 elements, termed nutrients to be able to photosynthesise. The availability of these nutrients in the upper  
60 ocean frequently limits the activity and abundance of these organisms together with light conditions  
61 (Moore et al., 2013). In particular, winter nutrient reserves in surface waters set an upper limit for  
62 biomass accumulation during the annual spring-to-summer bloom and will influence the duration of the  
63 bloom (Follows and Dutkiewicz, 2001; Henson et al., 2009; Moore et al., 2013; 2008). Hence, nutrient  
64 depletion due to biological consumption is considered as a major factor in the decline of blooms  
65 (Harrison et al., 2013).

66 The extensive studies conducted in the North Atlantic Ocean through the Continuous Plankton Recorder  
67 (CPR) have highlighted the relationship between the strength of the westerlies and the displacement of  
68 the subarctic front (SAF), (which corresponds to the North Atlantic Oscillation (NAO) index (Bersch et  
69 al., 2007)), and the phytoplankton dynamics of the central North Atlantic Ocean (Barton et al., 2003).  
70 Therefore, the SAF not only delineates the subtropical gyre from the subpolar gyre but also two distinct  
71 systems in which phytoplankton limitations are controlled by different factors. In the North Atlantic  
72 Ocean, spring phytoplankton growth is largely light-limited within the subpolar gyre. Light levels are  
73 primarily set by freeze-thaw cycles of sea ice and the high-latitude extremes in the solar cycle  
74 (Longhurst, 2007). Simultaneously, intense winter mixing supplies surface waters with high  
75 concentrations of nutrients. In contrast, within the subtropical gyre, the spring phytoplankton growth is  
76 less impacted by the light regime and has been shown to be N and P-co-limited (e.g. Harrison et al.,  
77 2013; Moore et al., 2008). This is principally driven by Ekman downwelling with an associated export of  
78 nutrients out of the euphotic zone (Oschlies, 2002). Thus, depending on the location of the SAF,  
79 phytoplankton communities from the central North Atlantic Ocean will be primarily light or nutrient  
80 limited.

81  
82 However, once the water column stratifies and phytoplankton are released from light limitation, seasonal  
83 high-nutrient, low chlorophyll (HNLC) conditions were reported at the transition zone between the gyres,  
84 especially in the Irminger Sea and Iceland Basin (Sanders et al., 2005). In these HNLC zones, trace  
85 metals are most likely limiting the biological carbon pump. Among all the trace metals, Fe has been  
86 recognized as the prime limiting element of North Atlantic primary productivity (e.g. Boyd et al., 2000;  
87 Martin et al., 1994; 1988; 1990). Indeed, Fe is a key element for a number of metabolic processes (e.g.  
88 Morel et al., 2008). However, the phytoplankton community has been shown to become N and/or Fe-  
89 (co)-limited in the Iceland Basin and the Irminger Sea (e.g. Nielsdóttir et al., 2009; Painter et al., 2014;  
90 Sanders et al., 2005).

91 In the North Atlantic Ocean, dissolved Fe (DFe) is delivered through multiple pathways such as ice-  
92 melting (e.g. Klunder et al., 2012; Tovar-Sanchez et al., 2010), atmospheric inputs (Achterberg et al.,  
93 2018; Baker et al., 2013; Shelley et al., 2015; 2017), coastal runoff (Rijkenberg et al., 2014), sediment  
94 inputs (Hatta et al., 2015), hydrothermal inputs (Achterberg et al., 2018; Conway and John, 2014) and  
95 by water mass circulation (vertical and lateral advections, e.g. Laes et al., 2003). Dissolved Fe can be  
96 regenerated through biological recycling (microbial loop, zooplankton grazing, e.g. Boyd et al., 2010;  
97 Sarthou et al., 2008). Iron is removed from the dissolved phase by biological uptake, export and  
98 scavenging throughout the water column and precipitation (itself a function of salinity, pH of seawater  
99 and ligand concentrations).

100 Although many studies investigated the distribution of DFe in the North Atlantic Ocean, much of this  
101 work was restricted to the upper layers (< 1000 m depth) or to one basin. Therefore, uncertainties remain  
102 on the large-scale distribution of DFe in the North Atlantic Ocean and more specifically within the  
103 subpolar gyre where few studies have been undertaken, and even fewer in the Labrador Sea. In this  
104 biogeochemically important area, high-resolution studies are still lacking for understanding the  
105 processes influencing the cycle of DFe.

106 The aim of this paper is to elucidate the sources and sinks of DFe, its distribution regarding water  
107 masses and assesses the links with biological activity along the GEOVIDE (GEOTRACES-GA01)  
108 transect. This transect spanned several biogeochemical provinces including the West European Basin,  
109 the Iceland Basin, the Irminger and the Labrador Seas (Fig. 1). In doing so we hope to constrain the  
110 potential long-range transport of DFe through the Deep Western Boundary Current (DWBC) via the  
111 investigation of the local processes effecting the DFe concentrations within the three main water masses

112 that constitute it: Iceland Scotland Overflow Water (ISOW), Denmark Strait Overflow Water (DSOW)  
113 and Labrador Sea Water (LSW).

114

## 115 **2 Material and methods**

116

### 117 **2.1 Study area and sampling activities**

118 Samples were collected during the GEOVIDE (GEOTRACES-GA01 section, Fig. 1) oceanographic  
119 voyage from 15 May 2014 (Lisbon, Portugal) to 30 June 2014 (St. John's, Newfoundland, Canada)  
120 aboard N/O *Pourquoi Pas?*. The study was carried out along the OVIDE line (<http://www.umr->  
121 [lops.fr/Projets/Projets-actifs/OVIDE](http://www.umr-lops.fr/Projets/Projets-actifs/OVIDE), previously referred to as the WOCE A25 Greenland to Portugal  
122 section), and in the Labrador Sea (corresponding to the WOCE A01 leg 3 Greenland to Newfoundland  
123 section). The OVIDE line has been sampled every two years since 2002 in the North Atlantic (e.g.  
124 Mercier et al., 2015), and in the Labrador Sea (broadly corresponding to the WOCE A01 leg 3 Greenland  
125 to Newfoundland section). In total, 32 stations were occupied, and samples were usually collected at 22  
126 depths, except at shallower stations close to the Iberian, Greenland and Canadian shelves (Fig. 1)  
127 where fewer samples (between 6 and 11) were collected. To avoid ship contamination of surface waters,  
128 the shallowest sampling depth was 15 m at all stations. Therefore, 'surface water samples' refers to  
129 15m depth.

130 Samples were collected using a trace metal clean polyurethane powder-coated aluminium frame rosette  
131 (hereafter referred to as TMR) equipped with twenty-two 12L, externally closing, Teflon-lined, GO-FLO  
132 bottles (General Oceanics) and attached to a Kevlar® line. The cleaning protocols for sampling bottles  
133 and equipment followed the guidelines of the GEOTRACES Cookbook ([www.geotraces.org](http://www.geotraces.org), Cutter et  
134 al., 2017). After TMR recovery, GO-FLO bottles were transferred into a clean container equipped with  
135 a class 100 laminar flow hood. Samples were either taken from the filtrate of particulate samples  
136 (collected on polyethersulfone filters, 0.45 µm supor®, see Gourain et al., 2019) or after filtration using  
137 0.2 µm filter cartridges (Sartorius SARTOBRAN® 300) due to water budget restriction (Table 1). Filtration  
138 techniques were not directly compared for the same samples, however, Wilcoxon statistical tests were  
139 performed to compare the distribution of DFe at each pair of adjacent stations where the change of  
140 filtration technique was performed (see Table 1). No significant differences were observed (p-value >  
141 0.2) for all pairs of stations (n = 9), except between stations 11/13 and 13/15. Moreover, both filtration  
142 techniques are deemed acceptable by the GEOTRACES guidelines. Seawater was collected in acid-

143 cleaned 60 mL LDPE bottles, after rinsing 3 times with about 20 mL of seawater. Teflon® tubing used to  
144 connect the filter holders or cartridges to the GO-FLO bottles were washed in an acid-bath (10% v/v  
145 HCl, Suprapur®, Merck) for at least 12 h and rinsed three times with Ultra High Purity Water (UHPW >  
146 18 MΩ.cm) prior to use. Samples were then acidified to ~ pH 1.7 with HCl (Ultrapur® Merck, 2 ‰ v/v)  
147 under a class 100 laminar flow hood inside the clean container. The sample bottles were then double  
148 bagged and stored at ambient temperature in the dark before shore-based analyses one year after  
149 collection.

150 Large volumes of seawater sample (referred hereafter as the in-house standard seawater) were also  
151 collected using a towed fish at around 2-3 m deep and filtered in-line inside a clean container through a  
152 0.2 µm pore size filter capsule (Sartorius SARTOBRAN® 300) and was stored unacidified in 20-30 L  
153 LDPE carboys (Nalgene™). All the carboys were cleaned following the guidelines of the GEOTRACES  
154 Cookbook (Cutter et al., 2017). This in-house standard seawater was used for calibration on the  
155 SeaFAST-pico™ - SF-ICP-MS (see Section 2.2) and was acidified to ~ pH 1.7 with HCl (Ultrapur® Merck,  
156 2 ‰ v/v) at least 24h prior to analysis.

157

## 158 **2.2 DFe analysis with SeaFAST-pico™**

159 Seawater samples were preconcentrated using a SeaFAST-pico™ (ESI, Elemental Scientific, USA) and  
160 the eluent was directly introduced via a PFA-ST nebulizer and a cyclonic spray chamber in an Element  
161 XR Sector Field Inductively Coupled Plasma Mass Spectrometer (Element XR SF-ICP-MS, Thermo  
162 Fisher Scientific Inc., Omaha, NE), following the protocol of Lagerström et al. (2013).

163 High-purity grade solutions and water (Milli-Q) were used to prepare the following reagents each day:  
164 the acetic acid-ammonium acetate buffer (CH<sub>3</sub>COO<sup>-</sup> and NH<sub>4</sub><sup>+</sup>) was made of 140 mL acetic acid (>  
165 99% NORMATOM® - VWR chemicals) and ammonium hydroxide (25%, Merck Suprapur®) in 500 mL  
166 PTFE bottles and was adjusted to pH 6.0 ± 0.2 for the on-line pH adjustment of the samples. The eluent  
167 was made of 1.4 M nitric acid (HNO<sub>3</sub>, Merck Ultrapur®) in Milli-Q water by a 10-fold dilution and spiked  
168 with 1 µg L<sup>-1</sup> <sup>115</sup>In (SCP Science calibration standards) to allow for drift correction. Autosampler and  
169 column rinsing solutions were made of HNO<sub>3</sub> 2.5% (v/v) (Merck Suprapur®) in Milli-Q water. The carrier  
170 solution driven by the syringe pumps to move the sample and buffer through the flow injection system  
171 was made in the same way.

172 All reagents, standards, samples, and blanks were prepared in acid cleaned low density polyethylene  
173 (LDPE) or Teflon fluorinated ethylene propylene (FEP) bottles. Bottles were cleaned following the  
174 GEOTRACES protocol (Cutter et al., 2017).  
175 Mixed element standard solution was prepared gravimetrically using high purity standards (Fe, Mn, Cd,  
176 Co, Zn, Cu, Pb; SCP Science calibration standards) in HNO<sub>3</sub> 3% (v/v) (Merck Ultrapur®). The  
177 distribution of the trace metals other than Fe will be reported elsewhere (Planquette et al., in prep.). A  
178 six-point calibration curve was prepared by standard additions of the mixed element standard to our  
179 acidified in-house standard and ran at the beginning, the middle and the end of each analytical session.  
180 Each analytical session consisted of about fifty samples. Final concentrations of samples and procedural  
181 blanks were calculated from In-normalized data. Data were blank-corrected by subtracting an average  
182 acidified Milli-Q blank that were pre-concentrated on the SeaFAST-pico™ in the same way as the  
183 samples and seawater standards. The errors associated to each sample were calculated as the  
184 standard deviation for five measurements of low-Fe seawater samples. The mean Milli-Q blank was  
185 equal to 0.08 ± 0.09 nmol L<sup>-1</sup> (n = 17) considering all analytical sessions. The detection limit, calculated  
186 for a given run as three times the standard deviation of the Milli-Q blanks, was on average 0.05 ± 0.05  
187 nmol L<sup>-1</sup> (n = 17). Reproducibility was assessed through the standard deviation of replicate samples  
188 (every 10th sample was a replicate) and the average of the in-house standard seawater, and was equal  
189 to 17% (n = 84). Accuracy was determined from the analysis of consensus (SAFe S, GSP) and certified  
190 (NASS-7) seawater matrices (see Table 2) and in-house standard seawater (DFe = 0.42 ± 0.07 nmol L<sup>-1</sup>,  
191 n = 84). Note that all the DFe values were generated in nmol kg<sup>-1</sup> using the SeaFAST-pico™ coupled  
192 to an Element XR SF-ICP-MS and were converted to nmol L<sup>-1</sup> using the actual density (in kg L<sup>-1</sup>) of each  
193 seawater sample (Table 1) to be directly comparable with literature.

194

### 195 **2.3 Meteoric water and sea ice fraction calculation**

196 We considered the different contributions of, Sea-Ice Melt (SIM), Meteoric Water (MW), and saline  
197 seawater, at Stations 53, 61 and 78 using the procedure and mass balance calculations that are fully  
198 described in Benetti et al. (2016). Briefly, we considered two types of seawater, namely Atlantic Water  
199 (AW) and Pacific Water (PW). The relative proportions of AW ( $f_{AW}$ ) and PW ( $f_{PW}$ ) are calculated based  
200 on the distinctive nitrogen to phosphorus (N-P) relationships for the two water masses (Jones et al.,  
201 1998) as follows (e.g. Sutherland et al., 2009):

202

$$f_{PW} = \frac{N^m - N^{AW}}{N^{PW} - N^{AW}} \text{ (eq.1)}$$

203 where is the measured dissolved inorganic nitrogen, and are the values for pure Atlantic and Pacific  
 204 water estimated from Jones et al. (1998), respectively, and values are calculated by substituting the  
 205  $PO_4^m$  value in the equation of the pure AW and PW N-P lines from Jones et al. (1998). However, during  
 206 GEOVIDE, the phosphate depleted near-surface values led to unrealistic lower than just below the  
 207 subsurface. Therefore, for all surface samples, the estimates were replaced by the values at 100 m.  
 208 Then, the surface values were adjusted by a factor of dilution proportional to the sample salinity.  
 209 After estimating  $f_{AW}$  and  $f_{PW}$  and their respective salinity and  $\delta^{18}O$  affecting each samples, the  
 210 contribution of SIM and MW can be determined using measured salinity ( $S_m$ ) and  $\delta^{18}O$  ( $\delta O_m^{18}$ ). The mass  
 211 balance calculations are presented below:

$$f_{AW} + f_{PW} + f_{MW} + f_{SIM} = 1 \text{ (eq.2)}$$

$$f_{AW} \cdot S_{AW} + f_{PW} \cdot S_{PW} + f_{MW} \cdot S_{MW} + f_{SIM} \cdot S_{SIM} = S_m \text{ (eq.3)}$$

$$f_{AW} \cdot \delta O_{AW}^{18} + f_{PW} \cdot \delta O_{PW}^{18} + f_{MW} \cdot \delta O_{MW}^{18} + f_{SIM} \cdot \delta O_{SIM}^{18} = \delta O_m^{18} \text{ (eq.4)}$$

216  
 217 where  $f_{AW}$ ,  $f_{PW}$ ,  $f_{MW}$ ,  $f_{SIM}$  are the relative fraction of AW, PW, MW, and SIM. To calculate the relative  
 218 fractions of AW, PW, MW and SIM we used the following end-members:  $S_{AW} = 35$ ,  $\delta O_{AW}^{18} = +0.18\text{‰}$   
 219 (Benetti et al., 2016);  $S_{PW} = 32.5$ ,  $\delta O_{PW}^{18} = -1\text{‰}$  (Cooper et al., 1997; Woodgate and Aagaard, 2005);  
 220  $S_{MW} = 0$ ,  $\delta O_{MW}^{18} = -18.4\text{‰}$  (Cooper et al., 2008);  $S_{SIM} = 4$ ,  $\delta O_{SIM}^{18} = +0.5\text{‰}$  (Melling and Moore, 1995).  
 221 Negative sea-ice fractions indicated a net brine release while positive sea-ice fractions indicated a net  
 222 sea-ice melting. Note that for stations over the Greenland Shelf, we assumed that Pacific Water (PW)  
 223 contribution was negligible for the calculations, supported by the very low PW fractions found at Cape  
 224 Farewell in May 2014 (see Figure B1 in Benetti et al., 2017), while for station 78, located on the  
 225 Newfoundland shelf, we used nutrient measurements to calculate the PW fractions, following the  
 226 approach from Jones et al. (1998) (the data are published in Benetti et al., 2017).

227

## 228 **2.4 Ancillary measurements and mixed layer depth determination**

229 Potential temperature ( $\theta$ ), salinity (S), dissolved oxygen ( $O_2$ ) and beam attenuation data were retrieved  
 230 from the CTD sensors (CTD SBE911 equipped with a SBE-43) that were deployed on a stainless steel  
 231 rosette. Salinity profiles were calibrated using 1228 samples taken from the GO-FLO bottles, leading to  
 232 a precision of 0.002 psu. The  $O_2$  data could not be directly calibrated with GO-FLO samples, due to a  
 233 the sampling time being too long, so the calibrated  $O_2$  profiles acquired by the classic CTD at the same



234 station were used to calibrate the O<sub>2</sub> profiles of the TMR CTD, with a precision estimated at 3 µmol/kg.  
235 Nutrient and total Chlorophyll-a (TChl-a) samples were collected using the classic CTD at the same  
236 stations as for the TMR. We used the data from the stainless steel rosette casts that were deployed  
237 immediately before or after our TMR casts. Pigments were separated and quantified following an  
238 adaptation of the method described by van Heukelem and Thomas (2001) and the analytical procedure  
239 used is described in Ras et al. (2008). The method adaptation allowed for higher sensitivity in the  
240 analysis of low phytoplankton biomass waters (see Ras et al., 2008). Briefly, frozen filters were extracted  
241 at -20°C in 3 mL of methanol (100%), sonicated and then clarified by vacuum filtration through Whatman  
242 GF/F filters. The total extraction time was 2 hours. The extracts were then analysed by HPLC with a  
243 complete Agilent Technologies system 1200 (comprising LC Chemstation software, a degasser, a binary  
244 pump, a refrigerated autosampler, a column thermostat and a diode array detector) when possible on  
245 the same day as extraction. The sample extracts were premixed (1:1) with a tetrabutylammonium  
246 acetate (TBAA) buffer solution (28 nM) prior to injection in the HPLC. The mobile phase was a mix  
247 between a solution (A) of TBAA 28 mM:methanol (30:70, v:v) and a solution (B) of 100% methanol (i.e.  
248 the organic solvent) with varying proportions during analysis. After elution, pigment concentrations (in  
249 mg m<sup>-3</sup>) were calculated according to Beer-Lambert's law (i.e.  $A = \epsilon LC$ ) from the peak areas with an  
250 internal standard correction (Vitamin E acetate, Sigma) and an external standard calibration (DHI Water  
251 and Environment, Denmark). This method allowed the detection of 23 phytoplankton pigments. The  
252 detection limits, defined as three times the signal:noise ratio for a filtered volume of 1 L, was 0.0001 mg  
253 m<sup>-3</sup> for total chlorophyll-a (TChl-a) and its injection precision was 0.91%  
254 All these data are available on the LEFE/CYBER database ([http://www.obs-  
255 vlfr.fr/proof/php/geovide/geovide.php](http://www.obs-vlfr.fr/proof/php/geovide/geovide.php)).  
256 The mixed layer depth ( $Z_m$ ) for each station was calculated using the function "calculate.mld" (part of  
257 the "rcalcofi" package, Ed Weber at NOAA SWFSC) created by Sam McClathie (NOAA Federal, 30<sup>th</sup>  
258 December 2013) for R software and where  $Z_m$  is defined as an absolute change in the density of  
259 seawater at a given temperature ( $\Delta\sigma_\theta \geq 0.125 \text{ kg m}^{-3}$ ) with respect to an approximately uniform region  
260 of density just below the ocean surface (Kara et al., 2000). In addition to the density criterion, the  
261 temperature and salinity profiles were inspected at each station for uniformity within this layer. When  
262 they were not uniform, the depth of any perturbation in the profile was chosen as the base of the  $Z_m$   
263 (Table 1).  
264

265 **2.5 Statistical analysis**

266 All statistical approaches, namely the comparison between the pore size used for filtration, correlations  
267 and Principal Component Analysis (PCA), were performed using the R statistical software (R  
268 development Core Team 2012). For all the results, p-values were calculated against the threshold value  
269 alpha ( $\alpha$ ), that we assigned at 0.05, corresponding to a 95% level of confidence. For all data sets, non-  
270 normal distributions were observed according to the Shapiro-Wilk test. Therefore, the significance level  
271 was determined with a Wilcoxon test.

272 All sections and surface layer plots were prepared using Ocean Data View (Schlitzer, 2016).

273

274 **2.6 Water mass determination and associated DFe concentrations**

275 The water mass structure in the North Atlantic Ocean from the GEOVIDE voyage was quantitatively  
276 assessed by means of an extended Optimum Multi-Parameter (eOMP) analysis with 14 water masses  
277 (for details see García-Ibáñez et al., 2015; this issue). Using this water mass determination, DFe  
278 concentrations were considered as representative of a specific water mass only when the contribution  
279 of this specific water mass was higher than 60% of the total water mass pool.

280

281 **2.7 Database**

282 The complete database of dissolved Fe is available in the electronic supplement  
283 [www.biogeosciences.net](http://www.biogeosciences.net). Overall, 540 data points of dissolved Fe are reported, among which 511  
284 values are used in this manuscript. The remaining 29 values (5.7% of the total dataset) are flagged as  
285 (suspect) outliers. These 29 outliers, flagged as “3” in the table, were not used in figures and in the  
286 interpretation of this manuscript. The criteria for rejection were based on the comparison with other  
287 parameters measured from the same GO-FLO sampler, and curve fitting versus samples collected  
288 above and below the suspect sample. The complete data set will be available in national and  
289 international databases (LEFE-CYBER, <http://www.obs-vlfr.fr/proof/index2.php>, and GEOTRACES  
290 <http://www.bodc.ac.uk/geotraces/>).

291

292

293 **3 Results**

294

295 **3.1 Hydrography**

296 The hydrology and circulation of the main water masses along the OVIDE section in the North Atlantic  
297 Subpolar Gyre and their contribution to the Atlantic Meridional Overturning Circulation (AMOC) have  
298 been described using an eOMP analysis by García-Ibáñez et al., (2015; 2018) and Zunino et al. (2017).  
299 For a schematic of water masses, currents and pathways, see Danialt et al. (2016). Hereafter we  
300 summarise the main features (Fig. 1 and 2).

301  
302 *Upper waters (~ 0 – 800 m)* - The cyclonic circulation of Eastern North Atlantic Central Water (ENACW)  
303 ( $12.3 < \theta < 16^{\circ}\text{C}$ ,  $35.66 < S < 36.2$ ,  $241 < O_2 < 251 \mu\text{mol kg}^{-1}$ ) occupied the water column from 0 to ~  
304 800 m depth from stations 1 to 25 representing 60% of the water mass pool. The sharp Subarctic Front  
305 (between stations 26 and 29), caused by the northern branch of the North Atlantic Current (NAC)  
306 separated the cyclonic subpolar from the anticyclonic subtropical gyre domains at  $50^{\circ}\text{N}$  and  $22.5^{\circ}\text{W}$ .  
307 ENACW were also encountered to a lesser extent and only in surface waters (from 0 to ~ 100 m depth)  
308 between stations 29 and 34 (representing less than 40% of the water mass pool). West of the Subarctic  
309 Front, Iceland SubPolar Mode Water (IcSPMW,  $7.07 < \theta < 8^{\circ}\text{C}$ ,  $35.16 < S < 35.23$ ,  $280 < O_2 < 289 \mu\text{mol}$   
310  $\text{kg}^{-1}$ ) was encountered from stations 34-40 (accounting for more than 45% of the water mass pool from  
311 0 to ~ 800 m depth) and Irminger SubPolar Mode Water (IrSPMW,  $\theta \approx 5^{\circ}\text{C}$ ,  $S \approx 35.014$ ) from stations  
312 42-44 (representing to 40% of the water mass pool from 0 to ~ 250 m depth) and stations 49 and 60  
313 (accounting for 40% of the water mass pool down to 1300 m depth). IcSPMW was also observed within  
314 the Subtropical gyre (stations 11-26), subducted below ENACW up to 1000 m depth. Stations 63 (> ~  
315 200 m depth) and 64 (from surface down to ~ 500 m depth) exhibited a contribution of the IrSPMW  
316 higher than 45%. Stations 44, 49 and 60, from the Irminger Sea, and 63 from the Labrador Sea were  
317 characterised by lower sea-surface salinity ranges ( $S = [34.636, 34.903]$ , stations 63 and 60,  
318 respectively), likely due to ice melting and meteoric water inputs. Subarctic Intermediate Water (SAIW,  
319  $4.5 < \theta < 6.0^{\circ}\text{C}$ ,  $34.70 < S < 34.80$ ) contributed to more than 40% of the water mass pool in the Iceland  
320 Basin between the surface and ~ 400 m depth at stations 29 and 32 and throughout the water column  
321 of stations 53, 56 and 61 and from surface down to ~ 200 m depth at station 63. From stations 68 to 78  
322 surface waters were characterized by a minimum of salinity and a maximum of oxygen ( $S = 34.91$ ,  $O_2$   
323  $= 285 \mu\text{mol kg}^{-1}$ ,  $\theta \approx 3^{\circ}\text{C}$ ) and corresponded to the newly formed Labrador Sea Water (LSW). The LSW  
324 was also observed in surface waters of station 44 with a similar contribution than IrSPMW (~ 40%).  
325

326 *Intermediate waters (~ 800 – 1400 m)* - Mediterranean Outflow Water (MOW), distinguishable from  
327 surrounding Atlantic Water by its high salinity tongue (up to 36.2), a minimum of oxygen ( $O_2 = 210 \mu\text{mol}$   
328  $\text{kg}^{-1}$ ) and relatively high temperatures (up to  $11.7^\circ\text{C}$ ) was observed from station 1 to 21 between 800  
329 and 1400 m depth at a neutral density ranging from 27.544 to 27.751  $\text{kg m}^{-3}$  with the maximum  
330 contribution to the whole water mass pool seen at station 1 ( $64 \pm 6\%$ ). Its main core was located at ~  
331 1200 m depth off the Iberian shelf from stations 1 to 11 and then gradually rising westward due to mixing  
332 with LSW within the North Atlantic subtropical gyre and a contribution of this water mass decreasing  
333 until station 21 down to 10-20%. LSW ( $27.763 < \text{neutral density} < 27.724 \text{ kg m}^{-3}$ ) was sourced from  
334 SPMW after intense heat loss and led to its deep convection. During GEOVIDE, LSW formed by deep  
335 convection the previous winter was found at several stations in the Labrador Sea (68, 69, 71 and 77).  
336 After convecting, LSW splits into three main branches with two main cores separated by the Reykjanes  
337 Ridge (stations 1-32, West European and Iceland Basins; stations 40-60, Irminger Sea), and the last  
338 one entering the West European Basin (Zunino et al., 2017).

339  
340 *Overflows and Deep waters (~ 1400 - 5500 m)* - North East Atlantic Deep Water (NEADW,  $1.98 < \theta <$   
341  $2.50^\circ\text{C}$ ,  $34.895 < S < 34.940$ ) was the dominant water mass in the West European Basin at stations 1-  
342 29 from 2000 m depth to the bottom and is characterized by high silicic acid ( $42 \pm 4 \mu\text{mol L}^{-1}$ ), nitrate  
343 ( $21.9 \pm 1.5 \mu\text{mol L}^{-1}$ ) concentrations and lower oxygen concentration ( $O_2 \approx 252 \mu\text{mol kg}^{-1}$ ) (see Sarthou  
344 et al., 2018). The core of the NEADW (stations 1-13) was located near the seafloor and gradually  
345 decreased westward. Polar Intermediate Water (PIW,  $\theta \approx 0^\circ\text{C}$ ,  $S \approx 34.65$ ) is a ventilated, dense, low-  
346 salinity water intrusion to the deep overflows within the Irminger and Labrador Seas that is formed at  
347 the Greenland shelf. PIW represents only a small contribution to the whole water mass pool (up to 27%)  
348 and was observed over the Greenland slope at stations 53 and 61 as well as in surface waters from  
349 station 63 (from 0 to ~ 200 m depth), in intermediate waters of stations 49, 60 and 63 (from ~ 500 to ~  
350 1500 m depth) and in bottom waters of stations 44, 68, 69, 71 and 77 with a contribution higher than  
351 10%. Iceland Scotland Overflow Water (ISOW,  $\theta \approx 2.6^\circ\text{C}$ ,  $S \approx 34.98$ ) is partly formed within the Arctic  
352 Ocean by convection of the modified Atlantic water. ISOW comes from the Iceland-Scotland sills and  
353 flows southward towards the Charlie-Gibbs Fracture Zone (CGFZ) and Bight Fracture Zone (BFZ)  
354 (stations 34 and 36) after which it reverses its flowing path northward and enters the Irminger Sea  
355 (stations 40 and 42) to finally reach the Labrador Sea close to the Greenland coast (station 49, station  
356 44 being located in between this two opposite flow paths). Along the eastern (stations 26-36) and

357 western (stations 40-44) flanks of the Reykjanes Ridge, ISOW had a contribution higher than 50% to  
358 the water mass pool. ISOW was observed from 1500 m depth to the bottom of the entire Iceland Basin  
359 (stations 29-38) and from 1800 to 3000 m depth within the Irminger Sea (stations 40-60). ISOW, despite  
360 having a fraction lower than 45% above the Reykjanes Ridge (station 38), was the main contributor to  
361 the water mass pool from 1300 m depth down to the bottom. ISOW was also observed within the  
362 Labrador Sea from stations 68 to 77. Finally, the deepest part of the Irminger (stations 42 and 44) and  
363 Labrador (stations 68-71) Seas were occupied by Denmark Strait Overflow Water (DSOW,  $\theta \approx 1.30^{\circ}\text{C}$ ,  
364  $S \approx 34.905$ ).

365

## 366 **3.2 Ancillary data**

367

### 368 **3.2.1 Nitrate**

369 Surface nitrate ( $\text{NO}_3^-$ ) concentrations (García-Ibáñez et al., 2018; Pérez et al., 2018; Sarthou et al.,  
370 2018) ranged from 0.01 to 10.1  $\mu\text{mol L}^{-1}$  (stations 53 and 63, respectively). There was considerable  
371 spatial variability in  $\text{NO}_3^-$  surface distributions with high concentrations found in the Iceland Basin and  
372 Irminger Sea (higher than 6  $\mu\text{mol L}^{-1}$ ), as well as at stations 63 (10.1  $\mu\text{mol L}^{-1}$ ) and 64 (5.1  $\mu\text{mol L}^{-1}$ ),  
373 and low concentrations observed in the West European Basin, in the Labrador Sea and above  
374 continental margins. The low surface concentrations in the West European Basin ranged from 0.02  
375 (station 11) to 3.9 (station 25)  $\mu\text{mol L}^{-1}$ . Station 26 delineating the extreme western boundary of the  
376 West European Basin exhibited enhanced  $\text{NO}_3^-$  concentrations as a result of mixing between ENACW  
377 and IcSPMW, although these surface waters were dominated by ENACW. In the Labrador Sea (stations  
378 68-78) low surface concentrations were observed with values ranging from 0.04 (station 68) to 1.8  
379 (station 71)  $\mu\text{mol L}^{-1}$ . At depth, the lowest concentrations (lower than 15.9  $\mu\text{mol L}^{-1}$ ) were measured in  
380 ENACW ( $\sim 0 - 800$  m depth) and DSOW ( $> 1400$  m depth), while the highest concentrations were  
381 measured within NEADW (up to 23.5  $\mu\text{mol L}^{-1}$ ), and in the mesopelagic zone of the West European and  
382 Iceland Basins (higher than 18.4  $\mu\text{mol L}^{-1}$ ).

383

### 384 **3.2.2 Chlorophyll-a**

385 Overall, most of the phytoplankton biomass was localised above 100 m depth with lower total  
386 chlorophyll-a (TChl-a) concentrations South of the Subarctic Front and higher at higher latitudes (see  
387 supplementary material Fig. S1). While comparing TChl-a maxima considering all stations, the lowest

388 value ( $0.35 \text{ mg m}^{-3}$ ) was measured within the West European Basin (station 19, 50 m depth) while the  
389 highest values were measured at the Greenland (up to  $4.9 \text{ mg m}^{-3}$ , 30 m depth, station 53 and up to  $6.6$   
390  $\text{mg m}^{-3}$ , 23 m depth, station 61) and Newfoundland (up to  $9.6 \text{ mg m}^{-3}$ , 30 m depth, station 78) margins.

391

### 392 **3.3 Dissolved Fe concentrations**

393 Dissolved Fe concentrations (see supplementary material Table S1) ranged from  $0.09 \pm 0.01 \text{ nmol L}^{-1}$   
394 (station 19, 20 m depth) to  $7.8 \pm 0.5 \text{ nmol L}^{-1}$  (station 78, 371 m depth) (see Fig. 3). Generally, vertical  
395 profiles of DFe for stations above the margins (2, 4, 53, 56, 61, and 78) showed an increase with depth,  
396 although sea-surface maxima were observed at stations 2, 4 and 56. For these margin stations, values  
397 ranged from 0.7 to  $1.0 \text{ nmol L}^{-1}$  in the surface waters. Concentrations increased towards the bottom,  
398 with more than  $7.8 \text{ nmol L}^{-1}$  measured at station 78, approximately  $1\text{-}3 \text{ nmol L}^{-1}$  for stations 2, 4, 53, and  
399 61, and just above  $0.4 \text{ nmol L}^{-1}$  for station 56 (Fig. 4). Considering the four oceanic basins, mean vertical  
400 profiles (supplementary material Fig. S2) showed increasing DFe concentrations down to 3000 m depth  
401 followed by decreasing DFe concentrations down to the bottom. Among deep-water masses, the lowest  
402 DFe concentrations were measured in the West European Basin. The Irminger Sea displayed the  
403 highest DFe concentrations from 1000 m depth to the bottom relative to other basins at similar depths  
404 (Fig. 3 and supplementary material Fig. S2). In the Labrador Sea, DFe concentrations were low and  
405 relatively constant at about  $0.87 \pm 0.06 \text{ nmol L}^{-1}$  from 250 m to 3000 m depth (Fig. S2). Overall, surface  
406 DFe concentrations were higher ( $0.36 \pm 0.18 \text{ nmol L}^{-1}$ ) in the North Atlantic Subpolar gyre (above  $52^\circ\text{N}$ )  
407 than in the North Atlantic Subtropical gyre ( $0.17 \pm 0.05 \text{ nmol L}^{-1}$ ). The surface DFe concentrations were  
408 generally smaller than  $0.3 \text{ nmol L}^{-1}$ , except for few stations in the Iceland Basin (stations 32 and 38),  
409 Irminger (stations 40 and 42) and Labrador (station 63) Seas, where values ranged between  $0.4\text{-}0.5$   
410  $\text{nmol L}^{-1}$ .

411

### 412 **3.4 DFe signatures in water masses**

413 In the Labrador Sea, IrSPMW exhibited an average DFe concentration of  $0.61 \pm 0.21 \text{ nmol L}^{-1}$  ( $n=14$ ).  
414 DFe concentrations in the LSW were the lowest in this basin, with an average value of  $0.71 \pm 0.27 \text{ nmol}$   
415  $\text{L}^{-1}$  ( $n=53$ ) (see supplementary material Fig. S3). Deeper, ISOW displayed slightly higher average DFe  
416 concentrations ( $0.82 \pm 0.05 \text{ nmol L}^{-1}$ ,  $n=2$ ). Finally, DSOW had the lowest average ( $0.68 \pm 0.06 \text{ nmol L}^{-1}$ ,  
417  $n=3$ , see supplementary material Fig. S3) and median ( $0.65 \text{ nmol L}^{-1}$ ) DFe values for intermediate and  
418 deep waters.

419 In the Irminger Sea, surface waters were composed of SAIW ( $0.56 \pm 0.24 \text{ nmol L}^{-1}$ ,  $n=4$ ) and IrSPMW  
420 ( $0.72 \pm 0.32 \text{ nmol L}^{-1}$ ,  $n=34$ ). The highest open-ocean DFe concentrations (up to  $2.5 \pm 0.3 \text{ nmol L}^{-1}$ ,  
421 station 44, 2600 m depth) were measured within this basin. In the upper intermediate waters, LSW was  
422 identified only at stations 40 to 44, and had the highest DFe values with an average of  $1.2 \pm 0.3 \text{ nmol L}^{-1}$   
423 ( $n=14$ ). ISOW showed higher DFe concentrations than in the Iceland Basin ( $1.3 \pm 0.2 \text{ nmol L}^{-1}$ ,  $n=4$ ).  
424 At the bottom, DSOW was mainly located at stations 42 and 44 and presented the highest average DFe  
425 values ( $1.4 \pm 0.4 \text{ nmol L}^{-1}$ ,  $n=5$ ) as well as the highest variability from all the water masses presented in  
426 this section (see supplementary material Fig. S3).  
427 In the Iceland Basin, SAIW and IcSPMW displayed similar averaged DFe concentrations ( $0.67 \pm 0.30$   
428  $\text{nmol L}^{-1}$ ,  $n=7$  and  $0.55 \pm 0.34 \text{ nmol L}^{-1}$ ,  $n=22$ , respectively). Averaged DFe concentrations were similar  
429 in both LSW and ISOW, and higher than in SAIW and IcSPMW ( $0.96 \pm 0.22 \text{ nmol L}^{-1}$ ,  $n=21$  and  $1.0 \pm$   
430  $0.3 \text{ nmol L}^{-1}$ ,  $n=10$ , respectively, see supplementary material Fig. S3).  
431 Finally, in the West European Basin, DFe concentrations in ENACW were the lowest of the whole  
432 section with an average value of  $0.30 \pm 0.16 \text{ nmol L}^{-1}$  ( $n=64$ ). MOW was present deeper in the water  
433 column but was not characterized by particularly high or low DFe concentrations relative to the  
434 surrounding Atlantic waters (see supplementary material Fig. S3). The median DFe value in MOW was  
435 very similar to the median value when considering all water masses ( $0.75$  and  $0.77 \text{ nmol L}^{-1}$ ,  
436 respectively, Fig. S3). LSW and IcSPMW displayed slightly elevated DFe concentrations compared to  
437 the overall median with mean values of  $0.82 \pm 0.08$  ( $n=28$ ) and  $0.80 \pm 0.04$  ( $n=8$ )  $\text{nmol L}^{-1}$ , respectively.  
438 The DFe concentrations in NEADW were relatively similar to the DFe median value of the GEOVIDE  
439 voyage ( $0.71$  and  $0.77 \text{ nmol L}^{-1}$ , respectively, Fig. S3).

440

441

#### 442 **4 Discussion**

443

444 In the following sections, we will first discuss the high DFe concentrations observed throughout the water  
445 column of stations 1 and 17 located in the West European Basin (Section 4.1), then, the relationship  
446 between water masses and the DFe concentrations (Section 4.2) in intermediate (Section 4.2.2 and  
447 4.2.3) and deep (Section 4.2.4 and 4.2.5) waters. We will also discuss the role of wind (Section 4.2.1),  
448 rivers (Section 4.3.1), meteoric water and sea-ice processes (Section 4.3.2), atmospheric deposition

449 (Section 4.3.3) and sediments (Section 4.4) in delivering DFe. Finally, we will discuss the potential Fe  
450 limitation using DFe:NO<sub>3</sub><sup>-</sup> ratios (Section 4.5).

451

#### 452 **4.1 High DFe concentrations at station 1 and 17**

453 Considering the entire section, two stations (stations 1 and 17) showed irregularly high DFe  
454 concentrations (> 1 nmol L<sup>-1</sup>) throughout the water column, thus suggesting analytical issues. However,  
455 these two stations were analysed twice and provided similar results, therefore discarding any analytical  
456 issues. This means that these high values originated either from genuine processes or from  
457 contamination issues. If there had been contamination issues, one would expect a more random  
458 distribution of DFe concentrations and less consistence throughout the water column. It thus appears  
459 that contamination issues were unlikely to happen. Similarly, the influence of water masses to explain  
460 these distributions was discarded as the observed high homogenized DFe concentrations were  
461 restricted to these two stations. Station 1, located at the continental shelf-break of the Iberian Margin,  
462 also showed enhanced PFe concentrations from lithogenic origin suggesting a margin source (Gourain  
463 et al., 2019). Conversely, no relationship was observed between DFe and PFe nor transmissometry for  
464 station 17. However, Ferron et al. (2016) reported a strong dissipation rate at the Azores-Biscay Rise  
465 (station 17) due to internal waves. The associated vertical energy fluxes could explain the homogenized  
466 profile of DFe at station 17, although such waves are not clearly evidenced in the velocity profiles.  
467 Consequently, the elevated DFe concentrations observed at station 17 remain unsolved.

468

#### 469 **4.2 DFe and hydrology keypoints**

470

##### 471 **4.2.1 How do Air-sea interactions affect DFe concentration in the Irminger Sea?**

472 Among the four distinct basins described in this paper, the Irminger Sea exhibited the highest DFe  
473 concentrations within the surface waters (from 0 to 250 m depth) with values ranging from 0.23 to 1.3  
474 nmol L<sup>-1</sup> for open-ocean stations. Conversely, low DFe concentrations were previously reported in the  
475 central Irminger Sea by Rijkenberg et al. (2014) (April-May, 2010) and Achterberg et al. (2018) (April-  
476 May and July-August, 2010) with DFe concentrations ranging from 0.11 to 0.15 and from ~ 0 to 0.14  
477 nmol L<sup>-1</sup>, respectively (see supplementary material Fig. S4 and Table S2). Differences might be due to  
478 the phytoplankton bloom advancement, the high remineralization rate (Lemaître et al., 2017) observed  
479 within the LSW in the Irminger Sea (see Section 4.1.3) and a deeper winter convection in early 2014.



480 Indeed, enhanced surface DFe concentrations measured during GEOVIDE in the Irminger Sea could  
481 be due to intense wind forcing events that would deepen the winter  $Z_m$  down to the core of the Fe-rich  
482 LSW.

483 In the North Atlantic Ocean, the warm and salty water masses of the upper limb of the MOC are  
484 progressively cooled and become denser, and subduct into the abyssal ocean. In some areas of the  
485 SubPolar North Atlantic, deep convective winter mixing provides a rare connection between surface and  
486 deep waters of the MOC thus constituting an important mechanism in supplying nutrients to the surface  
487 ocean (de Jong et al., 2012; Louanchi and Najjar, 2001). Deep convective winter mixing is triggered by  
488 the effect of wind and a pre-conditioning of the ocean in such a way that the inherent stability of the  
489 ocean is minimal. Pickart et al. (2003) demonstrated that these conditions are satisfied in the Irminger  
490 Sea with the presence of weakly stratified surface water, a close cyclonic circulation, which leads to the  
491 shoaling of the thermocline and intense winter air-sea buoyancy fluxes (Marshall and Schott, 1999).  
492 Moore (2003) and Piron et al. (2016) described low-altitude westerly jets centred northeast of Cape  
493 Farewell, over the Irminger Sea, known as tip jet events. These events occur when wind is split around  
494 the orographic features of Cape Farewell, and are strong enough to induce deep convective mixing  
495 (Bacon et al., 2003; Pickart et al., 2003). It has also been shown that during winters with a positive North  
496 Atlantic Oscillation (NAO) index, the occurrence of such events is favoured (Moore, 2003; Pickart et al.,  
497 2003), which was the case in the winter 2013-2014, preceding the GEOVIDE voyage as opposed to  
498 previous studies (Lherminier, pers. comm.). The winter mixed layer depth prior to the cruise reached up  
499 to 1200 m depth in the Irminger Sea (Zunino et al., 2017), which was most likely attributed to a final  
500 deepening due to wind forcing events (centred at station 44). Such winter entrainment was likely the  
501 process involved in the vertical supply of DFe within surface waters fuelling the spring phytoplankton  
502 bloom with DFe values close to those found in LSW.

503

#### 504 **4.2.2 Why don't we see a DFe signature in the Mediterranean Overflow Water (MOW)?**

505 On its northern shores, the Mediterranean Sea is bordered by industrialized European countries, which  
506 act as a continuous source of anthropogenic derived constituents into the atmosphere, and on the  
507 southern shores by the arid and desert regions of north African and Arabian Desert belts, which act as  
508 sources of crustal material in the form of dust pulses (Chester et al., 1993; Guerzoni et al., 1999; Martin  
509 et al., 1989). During the summer, when thermal stratification occurs, DFe concentrations in the SML can  
510 increase over the whole Mediterranean Sea by 1.6-5.3 nmol L<sup>-1</sup> in response to the accumulation of

511 atmospheric Fe from both anthropogenic and natural origins (Bonnet and Guieu, 2004; Guieu et al.,  
512 2010; Sarthou and Jeandel, 2001). After atmospheric deposition, the fate of Fe will depend on the nature  
513 of aerosols, Fe-ligand binding capacity, vertical mixing, biological uptake, and scavenging processes  
514 (Bonnet and Guieu, 2006; Wuttig et al., 2013). During GEOVIDE, MOW was observed at percentages  
515 higher than ~ 60% from stations 1 to 13 between 900 and 1100 m depth and associated with high  
516 dissolved aluminium (DAI, Menzel Barraqueta et al., 2018) concentrations (up to 38.7 nmol L<sup>-1</sup>),  
517 confirming the high atmospheric deposition in the Mediterranean region. In contrast to Al, no DFe  
518 signature was associated with MOW (Figs. 2 and 3). Using L-ADCP data during the cruise, we estimated  
519 a translation velocity for the MOW of ~ 3-8 cm s<sup>-1</sup>, consistent with previous published values (e.g. Armi  
520 et al., 1989; Schmidt et al., 1996). Our station 13 was located ~ 2000 km far from the origin of the MOW,  
521 which would mean a transit time of ~ 1-2 years. This transit time would allow the Fe signal to be  
522 preserved, when DFe residence times range from weeks to months in the surface waters and from tens  
523 to hundreds of years in deep waters (de Baar and de Jong, 2001; Sarthou et al., 2003; Croot et al.,  
524 2004; Bergquist and Boyle 2006; Gerringa et al 2015; Tagliabue et al., 2016). This feature was also  
525 reported in some studies (Hatta et al., 2015; Thuróczy et al., 2010), while others measured higher DFe  
526 concentrations in MOW (Gerringa et al., 2017; Sarthou et al., 2007). However, MOW coincides with the  
527 maximum Apparent Oxygen Utilization (AOU) and it is not possible to distinguish the MOW signal from  
528 the remineralisation signal (Sarthou et al., 2007). On the other hand, differences between studies are  
529 likely originating from the intensity of atmospheric deposition and the nature of aerosols. Indeed,  
530 Wagener et al. (2010) highlighted that large dust deposition events can accelerate the export of Fe from  
531 the water column through scavenging. As a result, in seawater with high DFe concentrations and where  
532 high dust deposition occurs, a strong individual dust deposition event could act as a sink for DFe. It thus  
533 becomes less evident to observe a systematic high DFe signature in MOW despite dust inputs.

534

#### 535 **4.2.3 Fe enrichment in Labrador Sea Water (LSW)**

536 As described in Section 3.1, the LSW exhibited increasing DFe concentrations from its source area, the  
537 Labrador Sea, toward the other basins with the highest DFe concentrations observed within the Irminger  
538 Sea, suggesting that the water mass was enriched in DFe either locally in each basin or during its flow  
539 path (see supplementary material Fig. S3). These DFe sources could originate from a combination of  
540 high export of PFe and its remineralisation in the mesopelagic area and/or the dissolution of sediment.

541 The Irminger and Labrador Seas exhibited the highest averaged integrated TChl-a concentrations ( $98$   
542  $\pm 32 \text{ mg m}^{-2}$  and  $59 \pm 42 \text{ mg m}^{-2}$ ) compared to the West European and Iceland Basins ( $39 \pm 10 \text{ mg m}^{-2}$   
543 and  $53 \pm 16 \text{ mg m}^{-2}$ ), when the influence of margins was discarded. Stations located in the Irminger  
544 (stations 40-56) and Labrador (stations 63-77) Seas, were largely dominated by diatoms (>50% of  
545 phytoplankton abundances) and displayed the highest chlorophyllide-a concentrations, a tracer of  
546 senescent diatom cells, likely reflecting post-bloom condition (Tonnard et al., in prep.). This is in line  
547 with the highest POC export data reported by Lemaitre et al. (2018) in these two oceanic basins. This  
548 likely suggests that biogenic PFe export was also higher in the Labrador and Irminger Seas than in the  
549 West European and Iceland Basins. In addition, Gourain et al. (2019) highlighted a higher biogenic  
550 contribution for particles located in the Irminger and Labrador Seas with relatively high PFe:PAI ratios  
551 ( $0.44 \pm 0.12 \text{ mol:mol}$  and  $0.38 \pm 0.10 \text{ mol:mol}$ , respectively) compared to particles from the West  
552 European and Iceland Basins ( $0.22 \pm 0.10$  and  $0.38 \pm 0.14 \text{ mol:mol}$ , respectively, see Fig. 6A in Gourain  
553 et al., 2019). However, they reported no difference in PFe concentrations between the four oceanic  
554 basins, when the influence of margins was discarded, which likely highlighted the remineralisation of  
555 PFe within the Irminger and Labrador Seas. Indeed, Lemaître et al. (2017) reported higher  
556 remineralisation rates within the Labrador (up to  $13 \text{ mmol C m}^{-2} \text{ d}^{-1}$ ) and Irminger Seas (up to  $10 \text{ mmol}$   
557  $\text{C m}^{-2} \text{ d}^{-1}$ ) using the excess barium proxy (Dehairs et al., 1997), compared to the West European and  
558 Iceland Basins (ranging from 4 to  $6 \text{ mmol C m}^{-2} \text{ d}^{-1}$ ). Therefore, the intense remineralisation rates  
559 measured in the Irminger and Labrador Seas likely resulted in enhanced DFe concentrations within  
560 LSW.

561 Higher DFe concentrations were, however, measured in the Irminger Sea compared to the Labrador  
562 Sea and coincided with lower transmissometry values (i.e. 98.0-98.5% vs. >99%), thus suggesting a  
563 particle load of the LSW. This could be explained by the reductive dissolution of Newfoundland Margin  
564 sediments. Indeed, Lambelet et al. (2016) reported high dissolved neodymium (Nd) concentrations (up  
565 to  $18.5 \text{ pmol.kg}^{-1}$ ) within the LSW at the edge of the Newfoundland Margin ( $45.73^\circ\text{W}$ ,  $51.82^\circ\text{N}$ ) as well  
566 as slightly lower Nd isotopic ratio values relative to those observed in the Irminger Sea. They suggested  
567 that this water mass had been in contact with sediments approximately within the last 30 years (Charette  
568 et al., 2015). Similarly, during GA03, Hatta et al. (2015) attributed the high DFe concentrations in the  
569 LSW to continental margin sediments. Consequently, it is also possible that the elevated DFe  
570 concentrations from the three LSW branches which entered the West European and Iceland Basins and

571 Irminger Sea was supplied through sediment dissolution (Measures et al., 2013) along the LSW  
572 pathway.

573 The enhanced DFe concentrations measured in the Irminger Sea and within the LSW were thus likely  
574 attributed to the combination of higher productivity, POC export and remineralisation as well as a DFe  
575 supply from reductive dissolution of Newfoundland sediments to the LSW along its flow path. Using  
576 temperature and salinity anomalies, Yashayaev et al. (2007) showed that the LSW reached the Irminger  
577 Sea and the Iceland Basin in 1-2 years and 4-5 years, respectively, after its formation in the Labrador  
578 Sea. The LSW transit time in this region is thus compatible with a DFe residence times (see above).

579

#### 580 **4.2.4 Enhanced DFe concentrations in the Irminger Sea bottom water**

581 Bottom waters from the Irminger Sea exhibited the highest DFe concentrations from the whole section,  
582 excluding the stations at the margins. Such a feature could be due to i) vertical diffusion from local  
583 sediment, ii) lateral advection of water mass(es) displaying enhanced DFe concentrations, and iii) local  
584 dissolution of Fe from particles. Hereafter, we discuss the plausibility of these three hypotheses.

585 The GEOTRACES GA02 voyage (leg 1, 64PE319) which occurred in April-May 2010 from Iceland to  
586 Bermuda sampled two stations north and south of our station 44 (~ 38.95°W, 59.62°N): station 5 (~  
587 37.91°W, 60.43°N) and 6 (~ 39.71°W, 58.60°N), respectively. High DFe concentrations in samples  
588 collected close to the bottom were also observed and attributed to sediment inputs highlighting boundary  
589 exchange between seawater and surface sediment (Lambelet et al., 2016; Rijkenberg et al., 2014).  
590 However, because a decrease in DFe concentrations was observed at our station 44 from 2500 m depth  
591 down to the bottom (Fig. 3 and Table S1), it appeared to be unlikely that these high DFe concentrations  
592 will be the result of local sediment inputs, as no DFe gradient from the deepest samples to those above  
593 was observed.

594 Looking at salinity versus depth for these three stations, one can observe the intrusion of Polar  
595 Intermediate Water (PIW) at station 44 during GEOVIDE, which was not observed during the GA02  
596 voyage and which contributed to about 14% of the water mass composition (García-Ibáñez et al., 2018)  
597 and might therefore be responsible for the high DFe concentrations (see supplementary material Fig.  
598 S5A). On the other hand, the PIW was also observed at station 49 (from 390 to 1240 m depth), 60 (from  
599 440 to 1290 m depth), 63 (from 20 to 1540 m depth), 68 (3340 m depth), 69 (from 3200 to 3440 m  
600 depth), 71 (from 2950 to 3440 m depth) and 77 (60 and 2500 m depth) with similar or higher contributions  
601 of the PIW without such high DFe concentrations (maximum DFe =  $1.3 \pm 0.1$  nmol L<sup>-1</sup>, 1240 m depth at

602 station 49). At this station, the DSOW relative abundance was more than 20% (Supp. Fig. S5). The  
603 overflow of this dense water in the Irminger Sea is associated with intense cyclonic boluses (Käse et  
604 al. 2003) and the entrainment of waters from the Greenland margin and slope by pulses of DSOW  
605 occurs all along its transport from Denmark Strait to the Greenland tip (Magaldi et al., 2011; von Appen  
606 et al., 2014). This phenomenon may enrich the DSOW with Fe as well as other elements. This was also  
607 observed for radium and actinium with a deviation from the conservative behaviour of  $^{226}\text{Ra}$  (Le Roy et  
608 al., 2018) and an increase of  $^{227}\text{Ac}$  activity at station 44 at 2500 m, reflecting inputs of these tracers.  
609 Therefore, the high DFe concentrations observed in the Irminger Sea might be inferred from substantial  
610 load of Fe-rich particles when DSOW is in contact with the Greenland margin.

611

#### 612 **4.2.5 Reykjanes Ridge: Hydrothermal inputs or Fe-rich seawater?**

613 Hydrothermal activity was assessed over the Mid Atlantic Ridge, namely the Reykjanes Ridge (RR),  
614 from stations 36 to 40. Indeed, within the interridge database (<http://www.interridge.org>), the Reykjanes  
615 Ridge is reported to have active hydrothermal sites. The sites were either confirmed (Baker and German,  
616 2004; German et al., 1994; Olafsson et al., 1991; Palmer et al., 1995) close to Iceland or inferred (e.g.  
617 Chen, 2003; Crane et al., 1997; German et al., 1994; Sinha et al., 1997; Smallwood and White, 1998)  
618 closer to the GEOVIDE section as no plume was detected but a high backscatter was reported  
619 potentially corresponding to a lava flow. Therefore, hydrothermal activity at the sampling sites remains  
620 unclear with no elevated DFe concentrations nor temperature anomaly above the ridge (station 38).  
621 However, enhanced DFe concentrations (up to  $1.5 \pm 0.22 \text{ nmol L}^{-1}$ , station 36, 2200 m depth) were  
622 measured east of the Reykjanes Ridge (Fig. 3). This could be due to hydrothermal activity and  
623 resuspension of sunken particles at sites located north of the section and transported through ISOW  
624 towards the section (Fig. 3). Indeed, Achterberg et al. (2018) highlighted at  $\sim 60^\circ\text{N}$  and over the  
625 Reykjanes Ridge a southward lateral transport of a Fe plume of up to 250-300 km. In agreement with  
626 these observations, previous studies (e.g. Fagel et al., 1996; Fagel et al., 2001; Lackschewitz et al.,  
627 1996; Parra et al., 1985) reported marine sediment mineral clays in the Iceland Basin largely dominated  
628 by smectite (> 60%), a tracer of hydrothermal alteration of basaltic volcanic materials (Fagel et al., 2001;  
629 Tréguer and De La Rocha, 2013). Kanzow and Zenk (2014) investigated the fluctuations of the ISOW  
630 plume around RR. The transit time, west of RR, between  $60^\circ\text{N}$  and the Bight Fracture Zone (BFZ) was  
631 around 5 months, compatible with the residence time of DFe (see above). Hence, the high DFe

632 concentrations measured east of RR could be due to a hydrothermal source and/or the resuspension of  
633 (basaltic) particles and their subsequent dissolution.  
634 West of the Reykjanes Ridge, a DFe-enrichment was also observed in ISOW at station 40 within the  
635 Irminger Sea (Fig. 3). The low transmissometer values within ISOW in the Irminger Sea (station 44)  
636 compared to the Iceland Basin (station 32) suggested a higher particle load (Fig. 4A in Gourain et al.,  
637 2019). These particles could come from the Bight Fracture Zone (BFZ, 56.91°N and 32.74°W) (Fig. 1)  
638 (Lackschewitz et al., 1996; Zou et al., 2017) since the transit time of the ISOW between BFZ and our  
639 station 40 is around 3 months (Kanzow and Zenk, 2014).

640

#### 641 **4.3 What are the main sources of DFe in surface waters?**

642 During GEOVIDE, enhanced DFe surface concentrations were observed at several stations (stations 1-  
643 4, 53, 61, 78) highlighting an external source of Fe to surface waters. The main sources able to deliver  
644 DFe to surface waters are riverine inputs, glacial inputs and atmospheric deposition. In the following  
645 sections, these potential sources of DFe to surface waters will be discussed.

646

##### 647 **4.3.1 Tagus riverine inputs**

648 Enhanced DFe surface concentrations (up to  $1.07 \pm 0.12 \text{ nmol L}^{-1}$ ) were measured over the Iberian  
649 Margin (stations 1-4) and coincided with salinity minima ( $\sim <35$ ) and enhanced DAI concentrations (up  
650 to  $31.8 \text{ nmol L}^{-1}$ , Menzel Barraqueta et al., 2018). DFe and DAI concentrations were both significantly  
651 negatively correlated with salinity ( $R^2 = \sim 1$  and  $0.94$ , respectively) from stations 1 to 13 (Fig. 5). Salinity  
652 profiles from station 1 to 4 showed evidence of a freshwater source with surface salinity ranging from  
653  $34.95$  (station 1) to  $35.03$  (station 4). Within this area, only two freshwater sources were possible: 1) wet  
654 atmospheric deposition (4 rain events, Shelley, pers. comm.) and 2) the Tagus River, since the ship  
655 SADCP data revealed a northward circulation with a velocity of around  $0.1 \text{ m/s}$  (P. Lherminier and P.  
656 Zunino, Ifremer Brest, pers. comm.). The transit time from the estuary to our stations above the shelf is  
657 around 15 days (150 km), which is short enough to preserve the DFe signal. Our SML DFe inventories  
658 were about three times higher at station 1 ( $\sim 1 \text{ nmol L}^{-1}$ ) than those calculated during the GA03 voyage  
659 ( $\sim 0.3 \text{ nmol L}^{-1}$ , station 1). Atmospheric deposition were about one order of magnitude higher during  
660 GA03 than during GA01 (Shelley et al., 2018; Shelley et al., 2015), thus the atmospheric source seemed  
661 to be minor during GA01. Consequently, the Tagus River appears as the most likely source responsible  
662 for these enhanced DFe concentrations, either as direct input of DFe or indirectly through Fe-rich

663 sediment carried by the Tagus River and their subsequent dissolution. The Tagus estuary is the largest  
664 in the western European coast and very industrialized (Canário et al., 2003; de Barros, 1986; Figueres  
665 et al., 1985; Gaudencio et al., 1991; Mil-Homens et al., 2009), that extends through an area of 320 km<sup>2</sup>  
666 and is characterized by a large water flow of 15.5 10<sup>9</sup> m<sup>3</sup> y<sup>-1</sup> (Fiuza, 1984). Many types of industry (e.g.  
667 heavy metallurgy, ore processing, chemical industry) release metals including Fe, which therefore result  
668 in high levels recorded in surface sediments, suspended particulate matter, water and organisms in the  
669 lower estuary (Santos-Echeandia et al., 2010).

670

#### 671 **4.3.2 High latitude meteoric water and sea-ice processes**

672 Potential sources of Fe at stations 53, 61 and 78 include meteoric water (MW, referring to precipitation,  
673 runoff and continental glacial melt), sea-ice melt (SIM), seawater interaction with shallow sediments and  
674 advection of water transported from the Arctic sourced by the Fe-rich TransPolar Drift (TPD, Klunder et  
675 al. (2012); see supplementary material Fig. S4 and Table S2). The vertical profiles of both potential  
676 temperature and salinity in the Greenland and Newfoundland Margins (station 53, 61 and 78, Fig. 4 D,  
677 E, and F) highlighted the presence of this freshwater lens likely originating from the Arctic Ocean. They  
678 were present in the upper 60 m (station 53) and 40 m (stations 61 and 78) depth. The most plausible  
679 source of this freshwater lens would be meteoric water and sea-ice melting. Deeper in the water column,  
680 net brine release (defined as a negative value of sea-ice melting) were observed at stations 53 (below  
681 40 m depth, Fig. 4D) 61 (in the whole water column, Fig. 4E) and 78 (below 30 m depth, Fig. 4F). The  
682 release of brines could originate from two different processes: the sea-ice formation or the early melting  
683 of multiyear sea ice due to gravitational drainage and subsequent brine release (Petrich and Eicken,  
684 2010; Wadhams, 2000). Indeed, during the winter preceding the GEOVIDE voyage, multiyear sea ice  
685 extended 200 km off the Greenland stations (<http://nsidc.org/arcticseaicenews/>). In the following  
686 sections, we discuss the potential for meteoric water supply, sea-ice formation and sea-ice melting to  
687 affect DFe distribution.

688

##### 689 *4.3.2.1 The Greenland shelf*

690 Considering the sampling period at stations 53 (16 June 2014) and 61 (19 June 2014), sea-ice formation  
691 is unlikely to happen as this period coincides with summer melting in both the Central Arctic and East  
692 Greenland (Markus et al., 2009). However, it is possible that the brines observed in our study could  
693 originate from sea-ice formation which occurred during the previous winter(s) at 66°N (and/or higher

694 latitudes). The brine signal at station 61 between 40 and 140 m was associated with a depletion in both  
695 DFe and PFe, which may be attributed to sea ice formation processes. Indeed, as soon as sea ice  
696 forms, sea salts are efficiently flushed out of the ice while PFe is trapped within the crystal matrix and  
697 DFe accumulates, leading to an enrichment factor of these two Fe fractions compared to underlying  
698 seawater (Janssens et al., 2016). Conversely, the strongest brine signal observed at station 53 (between  
699 50 and 160 m) showed slight enrichments in both DFe and PFe, which may be attributed to sea ice  
700 melting and the associated release into the underlying water column.

701 Surface waters at stations 53 and 61 were characterized by high MW fractions together with enrichments  
702 in PFe at station 53 and in both DFe and PFe at station 61 (Fig. 4D and E). These results are in line  
703 with previous observations, which highlighted strong inputs of DFe from a meteoric water melting source  
704 in Antarctica (Annett et al., 2015). At station 61, the relative depletion of DFe at 30 m compared to 50 m  
705 may be due to phytoplankton uptake, as indicated by the high TChl-a concentrations (up to  $6.6 \text{ mg m}^{-3}$ ,  
706 Fig. 4D). Hence, it seemed that meteoric water inputs from the Greenland Margin likely fertilized surface  
707 waters with DFe, enabling the phytoplankton bloom to subsist.

708

#### 709 *4.3.2.2 The Newfoundland shelf*

710 Newfoundland shelf waters (station 78) were characterized by high MW fractions (up to 7%), decreasing  
711 from surface to 200 m depth (~2%). These waters were associated with a net sea-ice melting signal  
712 from the near surface to ~10 m depth followed by a brine release signal down to 200 m depth with the  
713 maximum contribution measured at ~30 m depth. Within the surface waters (above 20 m depth), no  
714 elevation in DFe, DAI nor PFe was noticed despite the low measured TChl-a concentrations (TChl-a ~  
715  $0.20 \text{ mg m}^{-3}$ ). This suggests that none of these inputs (sea-ice melting and meteoric water) were able  
716 to deliver DFe or that these inputs were minor compared to sediment inputs from the Newfoundland  
717 Margin. Surprisingly, the highest TChl-a biomass (TChl-a >  $9 \text{ mg m}^{-3}$ ) from the whole section was  
718 measured at 30 m depth corresponding to the strongest brine release signal. This either suggests that  
719 the brine likely contained important amounts of Fe (dissolved and/or particulate Fe) that were readily  
720 available for phytoplankton and consumed at the sampling period by potentially sea-ice algae  
721 themselves (Riebesell et al., 1991) or that another nutrient was triggering the phytoplankton bloom.

722



723 **4.3.3 Atmospheric deposition**

724 On a regional scale, the North Atlantic basin receives the largest amount of atmospheric inputs due to  
725 its proximity to the Saharan Desert (Jickells et al., 2005), yet even in this region of high atmospheric  
726 deposition, inputs are not evenly distributed. Indeed, aerosol Fe loading measured during GEOVIDE  
727 (Shelley et al., 2017) were much lower (up to four orders of magnitude) than those measured during  
728 studies from lower latitudes in the North Atlantic (e.g. Baker et al., 2013; Buck et al., 2010; and for GA03,  
729 Shelley et al., 2015), but atmospheric inputs could still be an important source of Fe to surface waters  
730 in areas far from land.

731 In an attempt to estimate whether there was enough atmospheric input to sustain the SML DFe  
732 concentrations, we calculated Turnover Times relative to Atmospheric Deposition (TTADs, Guieu et al.,  
733 2014). To do so, we made the following assumptions: 1) the aerosol concentrations are a snapshot in  
734 time but are representative of the study region, 2) the aerosol solubility estimates based on two  
735 sequential leaches are an upper limit of the aerosol Fe in seawater and 3) the water column stratified  
736 just before the deposition of atmospheric inputs, so MLD DFe will reflect inputs from above. Thus, the  
737 TTADs were defined as the integrated DFe concentrations in the SML for each station divided by the  
738 contribution of soluble Fe contained in aerosols averaged per basin to the water volume of the SML.  
739 Although, TTADs were lower in the West European and Iceland Basins with an average of  $\sim 9 \pm 3$   
740 months compared to other basins ( $7 \pm 2$  years and  $5 \pm 2$  years for the Irminger and Labrador Seas,  
741 respectively) (Fig. 6) they were about three times higher than those reported for areas impacted by  
742 Saharan dust inputs ( $\sim 3$  months, Guieu et al., 2014). Therefore, the high TTADs measured in the  
743 Irminger and Labrador Seas and ranging from 2 to 15 years provided further evidence that atmospheric  
744 deposition were unlikely to supply Fe in sufficient quantity to be the main source of DFe (see Sections  
745 4.2.1 and 4.3.2) while in the West European and Iceland Basins they played an additional source,  
746 perhaps the main source of Fe especially at station 36 which displayed TTAD of 3 months.

747

748 **4.3.4 Sediment input**

749 *4.3.4.1 Margins:*

750 DFe concentration profiles from all coastal stations (stations 2, 4, 53, 56, 61 and 78) are reported in  
751 Figure 4. To avoid surface processes, only depths below 100 m depth will be considered in the following  
752 discussion. DFe and PFe followed a similar pattern at stations 2, 53, 56, and 78 with increasing  
753 concentrations towards the sediment, suggesting that either the sources of Fe supplied both Fe fractions

754 (dissolved and particulate) or that PFe dissolution from sediments supplied DFe. Among the different  
755 margins, the Newfoundland Margin exhibited the highest deep-water DFe and PFe concentrations.  
756 Conversely, stations 4 and 61 exhibited a decrease in DFe concentrations in the samples closest to the  
757 seafloor whereas PFe increased. DFe:PFe ratios ranged from 0.01 (station 2, bottom sample) to 0.27  
758 (station 4, ~ 400 m depth) mol:mol with an average value of  $0.11 \pm 0.07$  mol:mol ( $n = 23$ , Table 3). This  
759 could be explained by the different nature of the sediments and/or different sediment conditions (e.g.  
760 redox, organic content). Based on particulate and dissolved Fe and dissolved Al data (Gourain et al.,  
761 2019; Menzel Barraqueta et al., 2018, Table 3), three main different types of margins were reported  
762 (Gourain et al., 2019) with the highest lithogenic contribution observed at the Iberian Margin (stations 2  
763 and 4) and the highest biogenic contribution at the Newfoundland Margin (station 78). These  
764 observations are consistent with higher TChl-a concentrations measured at the Newfoundland Margin  
765 and to a lesser extent at the Greenland Margin and the predominance of diatoms relative to other  
766 functional phytoplankton classes at both margins (Tonnard et al., in prep.). To sum up, the more biogenic  
767 sediments (Newfoundland Margin) were able to mobilise more Fe in the dissolved phase than the more  
768 lithogenic sediments (Iberian Margin), in agreement with Boyd et al. (2010) who reported greater  
769 remineralization of PFe from biogenic PFe than from lithogenic PFe based on field experiment and  
770 modelling simulations.

771

#### 772 4.3.4.2 Nepheloid layers:

773 Samples associated with high levels of particles (transmissometer < 99%) and below 500 m depth  
774 displayed a huge variability in DFe concentrations. From the entire dataset, 63 samples (~13% of the  
775 entire dataset) followed this criterion with 14 samples from the West European Basin (station 1), 4  
776 samples from the Iceland Basin (stations 29, 32, 36 and 38), 43 samples from the Irminger Sea (stations  
777 40, 42, 44, 49 and 60) and 2 samples from the Labrador Sea (station 69). To determine which parameter  
778 was susceptible to explain the variation in DFe concentrations in these nepheloid layers, a Principal  
779 Component Analysis (PCA) on these samples. The input variables of the PCA were particulate Fe, Al,  
780 and particulate manganese (PMn) (Gourain et al., 2019), DAI (Menzel Barraqueta et al., 2018) and  
781 Apparent Oxygen Utilization (AOU) and were all correlated to DFe concentrations explaining all together  
782 93% of the subset variance (see supplementary material Fig. S6). The first dimension of the PCA was  
783 represented by PAI, PFe and PMn concentrations and explained 59.5% of the variance, while the  
784 second dimension was represented by the DAI and the AOU parameters, explaining 33.2% of the

785 variance. The two sets of variables were nearly at right angle from each other, indicating no correlation  
786 between them.

787 The variations in DFe concentrations measured in bottom samples from stations 32, 36 (Iceland Basin),  
788 42 and 44 (Irminger Sea) and 69 (Labrador Sea) were mainly explained by the first dimension of the  
789 PCA (see supplementary material Fig. S6). Therefore, samples characterized by the lowest DFe  
790 concentrations (stations 32 and 69) were driven by particulate Al and Mn concentrations and resulted  
791 in an enrichment of Fe in the particulate phase. These results are in agreement with previous studies  
792 showing that the presence of Mn within particles can induce the formation of Fe-Mn oxides, contributing  
793 to the removal of Fe and Mn from the dissolved phase (Kan et al., 2012; Teng et al., 2001).

794 Low DFe concentrations (bottom samples from stations 42 and 1) were linked to DAI inputs and  
795 associated with lower AOU values. The release of Al has previously been observed from Fe and Mn  
796 oxide coatings on resuspended sediments under mildly reducing conditions (Van Beusekom, 1988).  
797 Conversely, higher DFe concentrations were observed for stations 44 and 49 and to a lesser extent  
798 station 60 coinciding with low DAI inputs and higher oxygen levels. This observation challenges the  
799 traditional view of Fe oxidation with oxygen, either abiotically or microbially induced. Indeed,  
800 remineralisation can decrease sediment oxygen concentrations, promoting reductive dissolution of PFe  
801 oxyhydroxides to DFe that can then diffuse across the sediment water interface as DFe(II) colloids  
802 (Homoky et al., 2011). Such processes will inevitably lead to rapid Fe removal through precipitation of  
803 nanoparticulate or colloidal Fe (oxyhydr)oxides, followed by aggregation or scavenging by larger  
804 particles (Boyd and Ellwood, 2010; Lohan and Bruland, 2008) unless complexation with Fe-binding  
805 organic ligands occurs (Batchelli et al., 2010; Gerringa et al., 2008). There exist, however, another  
806 process that is favoured in oxic benthic boundary layers (BBL) with low organic matter degradation  
807 and/or low Fe oxides, which implies the dissolution of particles after resuspension, namely the non-  
808 reductive dissolution of sediment (Homoky et al., 2013; Radic et al., 2011). In addition, these higher  
809 oxygenated samples were located within DSOW, which mainly originate (75% of the overflow) from the  
810 Nordic Seas and the Arctic Ocean (Tanhua et al., 2005), in which the ultimate source of Fe was reported  
811 by Klunder et al. (2012) to come from Eurasian river waters. The major Arctic rivers were highlighted by  
812 Slagter et al. (2017) to be a source of Fe-binding organic ligands that are then further transported via  
813 the TPD across the Denmark Strait. Hence, the enhanced DFe concentrations measured within DSOW  
814 might result from Fe-binding organic ligand complexation that were transported to the deep ocean as  
815 DSOW formed rather than the non-reductive dissolution of sediment.

816

#### 817 **4.4 How does biological activity modify DFe distribution?**

818 Overall, almost all the stations from the GEOVIDE voyage displayed DFe minima in surface water  
819 associated with some maxima of TChl-*a* (see supplementary material Fig. S1). In the following section,  
820 we specifically address the question of whether DFe concentrations potentially limit phytoplankton  
821 growth. Note that macronutrients and DFe limitations relative to phytoplankton functional classes are  
822 dealt with Tonnard et al. (in prep.).

823 A key determinant for assessing the significance of a DFe source is the magnitude of the  
824 DFe:macronutrient ratio supplied, since this term determines to which extent DFe will be utilised. The  
825 DFe:NO<sub>3</sub><sup>-</sup> ratios in surface waters varied from 0.02 (station 36) to 38.6 (station 61) mmol:mol with an  
826 average of  $5 \pm 10$  mmol:mol (see supplementary material Fig. S7). Values were typically equal or lower  
827 than 0.28 mmol mol<sup>-1</sup> in all basins except at the margins and at stations 11, 13, 68, 69 and 77. The low  
828 nitrate concentrations observed at the eastern and western Greenland and Newfoundland Margins  
829 reflected a strong phytoplankton bloom which had reduced the concentrations as highlighted by the  
830 elevated integrated TChl-*a* concentrations ranging from 129.6 (station 78) to 398.3 (station 61) mg m<sup>-2</sup>.  
831 At the Iberian Margin, they likely reflected the influence of the N-limited Tagus River (stations 1, 2 and  
832 4) with its low TChl-*a* integrated concentrations that ranged from 31.2 (station 1) to 46.4 (station 4) mg  
833 m<sup>-2</sup>. The high DFe:NO<sub>3</sub><sup>-</sup> ratios determined at those stations, which varied from 13.4 (station 78) to 38.6  
834 (station 61) mmol:mol, suggested that waters from these areas, despite having the lowest NO<sub>3</sub><sup>-</sup>  
835 concentrations, were relatively enriched in DFe compared to waters from the Iceland Basin and the  
836 Irminger Sea.

837 In our study, DFe:NO<sub>3</sub><sup>-</sup> ratios displayed a gradient from the West European Basin to Greenland  
838 (supplementary material S7 and S8). This trend only reverses when the influence of Greenland was  
839 encountered, as also observed by Painter et al. (2014). The remineralisation of organic matter is a major  
840 source of macro and micronutrients in subsurface waters (from 50 to 250 m depth). Remineralisation is  
841 associated with the consumption of oxygen and therefore, Apparent Oxygen Utilization (AOU) can  
842 provide a quantitative estimate of the amount of material that has been remineralised. While no  
843 relationship was observed below 50 m depth for NO<sub>3</sub><sup>-</sup> or DFe and AOU considering all the stations, a  
844 significant correlation was found in the Subpolar gyre when removing the influence of margins (stations  
845 29-49, 56, 60, 63-77) ( $\text{AOU} = 3.65 \text{ NO}_3^- - 21.85$ ,  $R^2=0.70$ ,  $n=50$ ,  $p\text{-value} < 0.001$ ). This correlation  
846 indicates that remineralisation of Particulate Organic Nitrogen (PON) greatly translates into Dissolved

847 Inorganic Nitrogen (DIN) and that  $\text{NO}_3^-$  can be used as a good tracer for remineralisation in the studied  
848 area. Within these Subpolar gyre waters, there was a significant correlation between DFe and AOU  
849 ( $\text{AOU} = 23.92 \text{ DFe} + 10.45$ ,  $R^2=0.37$ ,  $n=58$ ,  $p\text{-value} < 0.001$ ). The open-ocean stations from the subpolar  
850 gyre also exhibited a good linear correlation between DFe and  $\text{NO}_3^-$  ( $\text{DFe} = 0.08 \text{ NO}_3^- - 0.48$ ,  $R^2=0.45$ ,  
851  $n=50$ ,  $p\text{-value} < 0.05$ ). (see supplementary material Fig. S8). The negative intercept of the regression  
852 line reflects possible excess of preformed  $\text{NO}_3^-$  compared to DFe in these water masses. These  
853 significant correlations allow us to use the  $\text{Fe}^*$  tracer to assess where DFe concentrations potentially  
854 limit phytoplankton growth by subtracting the contribution of organic matter remineralisation from the  
855 dissolved Fe pool, as defined by Rijkenberg et al. (2014) and Parekh et al. (2005) for  $\text{PO}_4^{3-}$ , and modified  
856 here for  $\text{NO}_3^-$  as follows:

$$857 \quad \text{Fe}^* = [\text{DFe}] - R_{\text{Fe:N}} \times [\text{NO}_3^-] \quad (\text{eq. 5})$$

858 where  $R_{\text{Fe:N}}$  refers to the average biological uptake ratio Fe over nitrogen, and  $[\text{NO}_3^-]$  refers to nitrate  
859 concentrations in seawater. Although, we imposed a fixed biological  $R_{\text{Fe:N}}$  of  $0.05 \text{ mmol mol}^{-1}$ , it is  
860 important to note that the biological uptake ratio of  $\text{DFe}:\text{NO}_3^-$  is not likely to be constant. Indeed, this  
861 ratio has been found to range from 0.05 to 0.9  $\text{mmol mol}^{-1}$  depending on species (Ho et al., 2003; Sunda  
862 and Huntsman, 1995; Twining et al., 2004). The ratio we choose is thus less drastic to assess potential  
863 Fe limitation and more representative of the average biological uptake of DFe over  $\text{NO}_3^-$  calculated for  
864 this study (i.e.  $R_{\text{Fe:N}} = 0.08 \pm 0.01 \text{ mmol mol}^{-1}$ , for Subpolar waters). Negative values of  $\text{Fe}^*$  indicate the  
865 removal of DFe that is faster than the input through remineralisation or external sources and positive  
866 values suggest input of DFe from external sources (Fig. 7). Consequently, figure 7 shows that  
867 phytoplankton communities with very high Fe requirements relative to  $\text{NO}_3^-$  ( $R_{\text{Fe:N}} = 0.9 \text{ mmol mol}^{-1}$ ) will  
868 only be able to grow above continental shelves where there is a high supply of DFe as previously  
869 reported by Nielsdóttir et al. (2009) and Painter et al. (2014). All these results are corroborating the  
870 importance of the Tagus River (Iberian Margin, see section 4.2.1), glacial inputs in the Greenland and  
871 Newfoundland Margins (see section 4.2.2) and to a lesser extent atmospheric inputs (see section 4.2.3)  
872 in supplying Fe with Fe:N ratios higher than the average biological uptake/demand ratio. Figure 7 (see  
873 also supplementary material S7, S9, S10 and S11) exhibits Fe:N ratios lower than  $0.05 \text{ mmol mol}^{-1}$ ,  
874 suggesting that Fe could also limit the low-Fe requirement phytoplankton class ( $R_{\text{Fe:N}} = 0.05 \text{ mmol mol}^{-1}$ )  
875 within the Iceland Basin, the Irminger, and the Labrador Seas. The Fe deficiency observed in surface  
876 waters ( $> 50 \text{ m}$  depth) from the Irminger and the Labrador Seas might be explained by low atmospheric  
877 deposition to ICSPMW and LSW (Shelley et al., 2017). Low atmospheric Fe supply and sub-optimal

878 Fe:N ratios in winter overturned deep water could favour the formation of the High-Nutrient, Low-  
879 Chlorophyll (HNLC) conditions. The West European Basin, despite exhibiting some of the highest  
880 DFe:NO<sub>3</sub><sup>-</sup> ratios within surface waters, displayed one of the strongest Fe-depletions from 50 m depth  
881 down to the bottom (see supplementary material Fig. S9 and S10), suggesting that the main source of  
882 Fe was coming from dust deposition and/or riverine inputs.

883 Similarly as for the West European Basin, the pattern displayed in the surface map of DFe:NO<sub>3</sub><sup>-</sup> ratios  
884 (supplementary material S9) extended to about 50 m depth, after which the trend reversed (Fig. 7 and  
885 supplementary material Fig. S7). Below 50 m depth, the Fe\* tracer (Fig. 7) was positive in the Irminger  
886 Sea and overall negative in the other basins. In the Irminger Sea positive Fe\* values were likely the  
887 result of the winter entrainment of Fe-rich LSW (see section 4.2.1) coinciding with high remineralised  
888 carbon fluxes in this area (station 44; Lemaître et al., 2017) (see section 4.2.2). The largest drawdown  
889 in DFe:NO<sub>3</sub><sup>-</sup> ratios was observed between stations 34 and 38 and was likely due to the intrusion of  
890 IcSPMW, this water mass exhibiting low DFe and high in NO<sub>3</sub><sup>-</sup> (from 7 to 8 µmol L<sup>-1</sup>) concentrations.  
891 Similarly, SAIW exhibited high NO<sub>3</sub><sup>-</sup> concentrations. Both the IcSPMW and the SAIW sourced from the  
892 NAC. The NAC as it flows along the coast of North America receives atmospheric depositions from  
893 anthropogenic sources (Shelley et al., 2017; 2015) which deliver high N relative to Fe (Jickells and  
894 Moore, 2015) and might be responsible for the observed ranges.

895

## 896 **5 Conclusion**

897 The DFe concentrations measured during this study were in good agreement with previous studies that  
898 spanned the West European Basin. However, within the Irminger Basin the DFe concentrations  
899 measured during this study were up to 3 times higher than those measured by Rijkenberg et al. (2014)  
900 in deep waters (> 1000 m depth). This is likely explained by the different water masses encountered  
901 (i.e. the Polar Intermediate Water, ~ 2800 m depth) and by a stronger signal of the Iceland Scotland  
902 Overflow Water (ISOW) from 1200 to 2300 m depth. This corresponded to the most striking feature of  
903 the whole section with DFe concentrations reaching up to 2.5 nmol L<sup>-1</sup> within ISOW, Denmark Strait  
904 Overflow Water (DSOW) and Labrador Sea Water (LSW), three water masses that are part of the Deep  
905 Western Boundary Current and was likely the result of a lateral advection of particles in the Irminger  
906 Sea. However, as these water masses reached the Labrador Sea, lower DFe levels were measured.  
907 These differences could be explained by different processes occurring within the benthic nepheloid  
908 layers, where DFe was sometimes trapped onto particles due to Mn-sediment within the Labrador Sea

909 (Gourain et al., 2019) and sometimes released from the sediment potentially as a result of interactions  
910 with dissolved organic matter. Such Fe-binding organic ligands could have also been produced locally  
911 due to the intense remineralisation rate reported by Lemaître et al. (2017) of biogenic particles (Boyd et  
912 al., 2010; Gourain et al., 2019). The LSW exhibited increasing DFe concentrations along its flow path,  
913 likely resulting from sediment inputs at the Newfoundland Margin. Although DFe inputs through  
914 hydrothermal activity were expected at the slow spreading Reykjanes Ridge (Baker and German, 2004;  
915 German et al., 1994), our data did not provide evidence of this specific source as previously suggested  
916 by Achterberg et al. (2018) at ~60°N.

917 In surface waters several sources of DFe were highlighted especially close to land, with riverine inputs  
918 from the Tagus River at the Iberian margin (Menzel Barraqueta et al., 2018) and meteoric inputs  
919 (including coastal runoff and glacial meltwater) at the Newfoundland and the Greenland margins (Benetti  
920 et al., 2016). Substantial sediment input was observed at all margins but with varying intensity. The  
921 highest DFe sediment input was located at the Newfoundland margin, while the lowest was observed at  
922 the eastern Greenland margin. These differences could be explained by the different nature of particles  
923 with the most lithogenic located at the Iberian margin and the most biogenic, at the Newfoundland  
924 margin (Gourain et al., 2019). Although previous studies (e.g. Jickells et al., 2005; Shelley et al., 2015)  
925 reported that atmospheric inputs substantially fertilized surface waters from the West European Basin,  
926 in our study, only stations located in the West European and Iceland Basins exhibited enhanced SML  
927 DFe inventories with lower TTADs. However, these TTADs were about three times higher than those  
928 reported for Saharan dust inputs and thus atmospheric deposition appeared to be a minor source of Fe  
929 during the sampling period. Finally, there was evidence of convective inputs of the LSW to surface  
930 seawater caused by long tip jet events (Piron et al., 2016) that deepened the winter mixed layer down  
931 to ~ 1200 m depth (Zunino et al., 2017), in which Fe was in excess of nitrate and therefore, Fe was not  
932 limiting.

933  
934 *Data availability.* All data are available on LEFE CYBER database at [http://www.obs-  
936 vlfr.fr/proof/php/geovide/x\\_datalist\\_1.php?xxop=geovide&xxcamp=geovide](http://www.obs-<br/>935 vlfr.fr/proof/php/geovide/x_datalist_1.php?xxop=geovide&xxcamp=geovide), and on request from the  
937 corresponding authors.

938 *Supplement.* The supplement related to this article is available online.  
939

940 *Author contributions.* MT, HP, and GS wrote this article with the advice and remarks of all the other co-  
941 authors. MG, FDP and YG accomplished the analyses of dissolved iron with the help of HP. MB and  
942 GR provided data and expertise for the Meteoric water and sea ice fraction calculation. AG and PT  
943 provided data and expertise for particulate iron and nutrient data, respectively. HP, JB, MC, FL, JLMB,  
944 LPC, and RS accomplished the sampling during the GEOVIDE cruise. The project was conceived and  
945 funded with the help of HP, PL, and GS.

946

947 *Competing interests.* The authors declare that they have no conflict of interest.

948

949 *Special issue statement.* This article is part of the special issue “GEOVIDE, an international  
950 GEOTRACES study along the OVIDE section in the North Atlantic and in the Labrador Sea (GA01)”. It  
951 is not associated with a conference.

952

953

954

#### 955 **Acknowledgements**

956 We are greatly indebted to the master, Gilles Ferrand, the officers and crew from the N/O *Pourquoi Pas?*  
957 for their logistic support during the GEOVIDE voyage. We would like to give a special thanks to Pierre  
958 Branellec, Michel Hamon, Catherine Kermabon, Philippe Le Bot, Stéphane Leizour, Olivier Ménage  
959 (Laboratoire d’Océanographie Physique et Spatiale), Fabien Pérault and Emmanuel de Saint Léger  
960 (Division Technique de l’INSU, Plouzané, France) for their technical expertise during clean CTD  
961 deployments as well as Emilie Grosteffan and Manon Le Goff for the analysis of nutrients. We also  
962 wanted to thank the Pôle Spectrométrie Océan (PSO, Plouzané, France) for letting us use the Element  
963 XR HR-ICP-MS. Greg Cutter is also strongly acknowledged for his help in setting up the new French  
964 clean sampling system. Catherine Schmechtig is thanked for the LEFE-CYBER database management.  
965 This work was funded by the French National Research Agency ANR GEOVIDE (ANR-13-BS06-0014)  
966 and RPDOC BITMAP (ANR-12-PDOC-0025-01), the French National Center for Scientific Research  
967 (CNRS-LEFE-CYBER), the LabexMER (ANR-10-LABX-19) and Ifremer and was supported for the  
968 logistic by DT-INSU and GENAVIR. Manon Tonnard was supported by a cotutelle joint PhD scholarship  
969 from the Université de Bretagne Occidentale (UBO-IUEM) and the University of Tasmania (UTAS-  
970 IMAS).



971

972 All dissolved iron (DFe) data are available in the supplementary material S1.

973

974

975

976 **References**

977 Achterberg, E. P., Steigenberger, S., Marsay, C. M., LeMoigne, F. A., Painter, S. C., Baker, A. R., Connelly, D. P.,  
978 Moore, C. M., Tagliabue, A., and Tanhua, T.: Iron Biogeochemistry in the High Latitude North Atlantic Ocean,  
979 Scientific reports, 8, 1-15, 10.1038/s41598-018-19472-1, 2018.

980 Aminot, A., and Kerouel, R.: Dosage automatique des nutriments dans les eaux marines, Quae ed., 2007.

981 Annett, A. L., Skiba, M., Henley, S. F., Venables, H. J., Meredith, M. P., Statham, P. J., and Ganeshram, R. S.:  
982 Comparative roles of upwelling and glacial iron sources in Ryder Bay, coastal western Antarctic Peninsula,  
983 Marine Chemistry, 176, 21-33, 10.1016/j.marchem.2015.06.017, 2015.

984 Armi, L., Hebert, D., Oakey, N., Price, J., Richardson, P. L., Rossby, T. and Ruddick, B.: The history and decay of  
985 a Mediterranean salt lens, Nature, 333(6174), 649–651, doi:10.1038/333649a0, 1988.

986 Bacon, S., Gould, W. J., and Jia, Y.: Open-ocean convection in the Irminger Sea, Geophysical Research Letters,  
987 30, 1246, doi:10.1029/2002GL016271, 2003.

988 Baker, A. R., Adams, C., Bell, T. G., Jickells, T. D., and Ganzeveld, L.: Estimation of atmospheric nutrient inputs to  
989 the Atlantic Ocean from 50°N to 50°S based on large-scale field sampling: Iron and other dust-associated  
990 elements, Global Biogeochemical Cycles, 27, 755-767, 10.1002/gbc.20062, 2013.

991 Baker, A. T., and German, C. R.: On the Global Distribution of Hydrothermal vent Fields, . In Mid-Ocean Ridges:  
992 Hydrothermal Interactions Between the Lithosphere and Oceans, Geophysical Monograph Series 148, C.R.  
993 German, J. Lin, and L.M. Parson (eds.), 245–266 (2004)

994

995 Barton, A. D., Greene, C. H., Monger, B. C., and Pershing, A. J.: The Continuous Plankton Recorder survey and  
996 the North Atlantic Oscillation: Interannual- to Multidecadal-scale patterns of phytoplankton variability in the North  
997 Atlantic Ocean, Progress in Oceanography, 58, 337-358, 10.1016/j.pocean.2003.08.012, 2003.

998 Batchelli, S., Muller, F. L. L., Chang, K. C., and Lee, C. L.: Evidence for Strong but Dynamic Iron-Humic Colloidal  
999 Associations in Humic-Rich Coastal Waters., Environmental Science & Technology, 44, 8485-8490,  
1000 <https://doi.org/10.1021/es101081c>, 2010.

1001 Benetti, M., Reverdin, G., Pierre, C., Khatiwala, S., Tournadre, B., Olafsdottir, S., and Naamar, A.: Variability of sea  
1002 ice melt and meteoric water input in the surface Labrador Current off Newfoundland, Journal of Geophysical  
1003 Research Oceans, 121, 2841-2855, doi:10.1002/2015JC011302., 2016.

1004 Benetti, M., Reverdin, G., Lique, C., Yashayaev, I., Holliday, N. P., Tynan, E., Torres-Valdes, S., Lherminier, P.,  
1005 Tréguer, P., and Sarthou, G.: Composition of freshwater in the spring of 2014 on the southern Labrador shelf  
1006 and slope, *Journal of Geophysical Research: Oceans*, 122, 1102-1121, 10.1002/2016jc012244, 2017.

1007 Bergquist, B. A. and Boyle, E. A.: Dissolved iron in the tropical and subtropical Atlantic Ocean, *Global*  
1008 *Biogeochemical Cycles*, 20(1), doi:10.1029/2005GB002505, 2006.

1009 Bersch, M., Yashayaev, I., and Koltermann, K. P.: Recent changes of the thermohaline circulation in the subpolar  
1010 North Atlantic, *Ocean Dynamics*, 57, 223-235, 10.1007/s10236-007-0104-7, 2007.

1011 Bhatia, M. P., Kujawinski, E. B., Das, S. B., Breier, C. F., Henderson, P. B., and Charette, M. A.: Greenland  
1012 meltwater as a significant and potentially bioavailable source of iron to the ocean, *Nature Geoscience*, 2013,  
1013 274-278, 10.1038/ngeo1746, 2013.

1014 Bonnet, S., and Guieu, C.: Dissolution of atmospheric iron in seawater, *Geophysical Research Letters*, 31,  
1015 10.1029/2003gl018423, 2004.

1016 Bonnet, S., and Guieu, C.: Atmospheric forcing on the annual iron cycle in the western Mediterranean Sea: A 1-  
1017 year survey, *Journal of Geophysical Research*, 111, 10.1029/2005jc003213, 2006.

1018 Boyd, P. W., Watson, A. J., Law, C. S., Abraham, E. R., Trull, T., Murdoch, R., Bakker, D. C. E., Bowie, A. R.,  
1019 Buesseler, K. O., Chang, H., Charette, M., Croot, P., Downing, K., Frew, R., Gall, M., Hadfield, M., Hall, J.,  
1020 Harvey, M., Jameson, G., LaRoche, J., Liddicoat, M., Ling, R., Maldonado, M. T., McKay, R. M., Nodder, S.,  
1021 Pickmere, S., Pridmore, R., Rintoul, S., Safi, K., Sutton, P., Strzepek, R., Tanneberger, K., Turner, S., Waite,  
1022 A., and Zeldis, J.: A mesoscale phytoplankton bloom in the polar Southern Ocean stimulated by iron fertilization,  
1023 *Nature*, 407, 695-702, 10.1038/35037500, 2000.

1024 Boyd, P. W., and Ellwood, M. J.: The biogeochemical cycle of iron in the ocean, *Nature Geoscience*, 3, 675-682,  
1025 10.1038/ngeo964, 2010.

1026 Boyd, P. W., Ibsanmi, E., Sander, S. G., Hunter, K. A., and Jackson, G. A.: Remineralization of upper ocean  
1027 particles: Implications for iron biogeochemistry, *Limnology and Oceanography*, 55, 1271-1288,  
1028 10.4319/lo.2010.55.3.1271, 2010.

1029 Buck, C. S., Landing, W. M., Resing, J. A., and Measures, C. I.: The solubility and deposition of aerosol Fe and  
1030 other trace elements in the North Atlantic Ocean: Observations from the A16N CLIVAR/CO2 repeat hydrography  
1031 section, *Marine Chemistry*, 120, 57-70, 10.1016/j.marchem.2008.08.003, 2010.

1032 Canário, J., Vale, C., Caetano, M., and Madureira, M. J.: Mercury in contaminated sediments and pore waters  
1033 enriched in sulphate (Tagus Estuary, Portugal), *Environmental Pollution*, 126, 425-433, 10.1016/S0269-  
1034 7491(03)00234-3, 2003.

1035 Charette, M. A., Morris, P. J., Henderson, P. B., and Moore, W. S.: Radium isotope distributions during the US  
1036 GEOTRACES North Atlantic cruises, *Marine Chemistry*, 177, 184-195, 10.1016/j.marchem.2015.01.001, 2015.

1037 Chen, Y. J.: Influence of the Iceland mantle plume on crustal accretion at the inflated Reykjanes Ridge: Magma  
1038 lens and low hydrothermal activity, *Journal of Geophysical Research*, 108, 2524, [https://doi-  
1040 org.inee.bib.cnrs.fr/10.1029/2001JB000816](https://doi-<br/>
1039 org.inee.bib.cnrs.fr/10.1029/2001JB000816), 2003.

1041 Chester, R., Murphy, K. J. T., Lin, F. J., Berry, A. S., Bradshaw, G. A., and Corcoran, P. A.: Factors controlling the  
1042 solubilities of trace-metals from nonremote aerosols deposited to the sea-surface by the dry deposition mode,  
1043 *Marine Chemistry*, 42, 107-126, 10.1016/0304-4203(93)90241-f, 1993.

1044 Conway, T. M., and John, S. G.: Quantification of dissolved iron sources to the North Atlantic Ocean, *Nature*, 511,  
1045 212-215, 10.1038/nature13482, 2014.

1046 Cooper, L. W., Whittedge, T. E., Grebmeier, J. M., and Weingartner, T.: The nutrient, salinity, and stable oxygen  
1047 isotope composition of Bering and Chukchi Seas waters in and near the Bering Strait, *Journal of Geophysical  
1048 Research*, 102, 12,563-512,573, 1997.

1049 Cooper, L. W., McClelland, J. W., Holmes, R. M., Raymond, P. A., Gibson, J. J., Guay, C. K., and Peterson, B. J.:  
1050 Flow-weighted values of runoff tracers ( $\delta^{18}\text{O}$ , DOC, Ba, alkalinity) from the six largest Arctic rivers, *Geophysical  
1051 Research Letters*, 35, 1-5, 10.1029/2008GL035007, 2008.

1052 Crane, K., Johnson, L., Appelgate, B., Nishimura, C., Buck, R., Jones, C., Vogt, P., and Kos'yan, R. Volcanic and  
1053 Seismic Swarm Events on the Reykjanes Ridge and Their Similarities to Events on Iceland: Results of a Rapid  
1054 Response Mission. *Marine Geophysical Researches (1997)* 19: 319. <https://doi.org/10.1023/A:1004298425881>

1055 Croot, P. L., Streu, P. and Baker, A. R.: Short residence time for iron in surface seawater impacted by atmospheric  
1056 dry deposition from Saharan dust events, *Geophys. Res. Lett.*, 31(L23S08), doi: 10.1029/2004GL020153, 2004.

1057 Cutter, G., Casciotti, K., Croot, P., Geibert, W., Heimbürger, L. E., Lohan, M., Planquette, H., and van de Fliedert,  
1058 T.: Sampling and the Sample-handling Protocols for GEOTRACES Cruises, 2017.

1059 Daniault, N., Mercier, H., Lherminier, P., Sarafanov, A., Falina, A., Zunino, P., Pérez, F. F., Ríos, A. F., Ferron, B.,  
1060 Huck, T., Thierry, V., and Gladyshev, S.: The northern North Atlantic Ocean mean circulation in the early 21st  
1061 century, *Progress in Oceanography*, 146, 142-158, 10.1016/j.pocean.2016.06.007, 2016.

1062 de Baar, H. J. W. and de Jong, J. T. M.: Distributions, Sources and Sinks of Iron in Seawater, in *Biogeochemistry  
1063 of Fe in Seawater*, vol. Chapter 5, edited by D. R. Turner and K. A. Hunter, pp. 123–253, SCOR-IUPAC series,  
1064 J Wiley, Baltimore., 2001.

1065 de Barros, M. C.: A case study of waste inputs in the Tagus estuary, in: *The role of the Oceans as a Waste Disposal  
1066 Option*, edited by: Kullenberg, G., NATO ASI Series; Series C: Mathematical and Physical Sciences, 172,  
1067 Springer Netherlands, 307-324, 1986.

1068 de Jong, M. F., van Aken, H. M., Våge, K., and Pickart, R. S.: Convective mixing in the central Irminger Sea: 2002–  
1069 2010, *Deep Sea Research Part I: Oceanographic Research Papers*, 63, 36-51, 10.1016/j.dsr.2012.01.003,  
1070 2012.

1071 Dehairs, F., Shopova, D., Ober, S., Veth, C., and Goeyens, L.: Particulate barium stocks and oxygen consumption  
1072 in the Southern Ocean mesopelagic water column during spring and early summer: Relationship with export  
1073 production, *Deep Sea Research II*, 44, 497-516, 10.1016/S0967-0645(96)00072-0, 1997.

1074 Deng, F., Henderson, G. M., Castrillejo, M., and Perez, F. F.: Evolution of <sup>231</sup>Pa and <sup>230</sup>Th in overflow waters of the  
1075 North Atlantic, *Biogeosciences*, 15, 7299–7313, <https://doi.org/10.5194/bg-15-7299-2018>, 2018.

1076 Fagel, N., Robert, C., and Hilaire-Marcel, C.: Clay mineral signature of the NW Atlantic Boundary Undercurrent,  
1077 *Marine Geology*, 130, 19-28, [https://doi.org/10.1016/0025-3227\(95\)00134-4](https://doi.org/10.1016/0025-3227(95)00134-4), 1996.

1078 Fagel, N., Robert, C., Preda, M., and Thorez, J.: Smectite composition as a tracer of deep circulation: the case of  
1079 the Northern North Atlantic, *Marine Geology*, 172, 309-330, [https://doi.org/10.1016/S0025-3227\(00\)00123-7](https://doi.org/10.1016/S0025-3227(00)00123-7),  
1080 2001.

1081 Ferron, B., Kokoszka, F., Mercier, H., Lherminier, P., Huck, T., Rios, A., and Thierry, V.: Variability of the Turbulent  
1082 Kinetic Energy Dissipation along the A25 Greenland–Portugal Transect Repeated from 2002 to 2012, *Journal*  
1083 *of Physical Oceanography*, 46, 1989-2003, 10.1175/jpo-d-15-0186.1, 2016.

1084 Figueres, G., Martin, J. M., Meybeck, M., and Seyler, P.: A comparative study of mercury contamination in the  
1085 Tagus estuary (Portugal) and major French estuaries (Gironde, Loire, Rhone), *Estuarine, Coastal and Shelf*  
1086 *Science*, 20, 183-203, [https://doi.org/10.1016/0272-7714\(85\)90037-X](https://doi.org/10.1016/0272-7714(85)90037-X), 1985.

1087 Fiuza, A.: Hidrologia e dinamica das aguas costeiras de Portugal, Ph. D., Universidade de Lisboa, Lisboa, Portugal,  
1088 unpublished, 1984.

1089 Follows, M., and Dutkiewicz, S.: Meteorological modulation of the North Atlantic Spring Bloom, *Deep Sea Research*  
1090 *Part II: Topical Studies in Oceanography*, 49, 321-344, [https://doi.org/10.1016/S0967-0645\(01\)00105-9](https://doi.org/10.1016/S0967-0645(01)00105-9), 2001.

1091 García-Ibáñez, M. I., Pardo, P. C., Carracedo, L. I., Mercier, H., Lherminier, P., Ríos, A. F., and Pérez, F. F.:  
1092 Structure, transports and transformations of the water masses in the Atlantic Subpolar Gyre, *Progress in*  
1093 *Oceanography*, 135, 18-36, 10.1016/j.pocean.2015.03.009, 2015.

1094 García-Ibáñez, M. I., Pérez, F. F., Lherminier, P., Zunino, P., Mercier, H., and Tréguer, P.: Water mass distributions  
1095 and transports for the 2014 GEOVIDE cruise in the North Atlantic, *Biogeosciences*, 15, 2075-2090, 10.5194/bg-  
1096 15-2075-2018, 2018.

1097 Gaudencio, M. J., Guerra, M. T., and Glemarec, M.: Recherches biosédimentaires sur la zone maritime de l'estuaire  
1098 du Tage, Portugal: données sédimentaires préliminaires. , in: *Estuaries and Coasts: Spatial and Temporal*  
1099 *Intercomparisons*, edited by: Elliot, M., and Ducrotoy, J. C., Olsen and Olsen, Fredensborg, 11-16, 1991.

1100 German, C. R., Briem, J., Chin, C. S., Danielsen, M., Holland, S., James, R. H., Jonsdottir, A., Ludford, E., Moser,  
1101 C., Olafsson, J., Palmer, M. R., and Rudnicki, M. D.: Hydrothermal activity on the Reykjanes Ridge: the  
1102 Steinahóll vent-field at 63°06'N, *Earth and Planetary Science Letters*, 121, 647-654,  
1103 [https://doi.org/10.1016/0012-821X\(94\)90098-1](https://doi.org/10.1016/0012-821X(94)90098-1), 1994.

1104 Gerringa, L. J. A., Blain, S., Laan, P., Sarthou, G., Veldhuis, M. J. W., Brussaard, C. P. D., Viollier, E., and  
1105 Timmermans, K. R.: Fe-binding dissolved organic ligands near the Kerguelen Archipelago in the Southern

1106 Ocean (Indian sector), *Deep Sea Research Part II: Topical Studies in Oceanography*, 55, 606-621,  
1107 10.1016/j.dsr2.2007.12.007, 2008.

1108 Gerringa, L. J. A., Rijkenberg, M. J. A., Schoemann, V., Laan, P. and de Baar, H. J. W.: Organic complexation of  
1109 iron in the West Atlantic Ocean, *Marine Chemistry*, 177, 434–446, doi:10.1016/j.marchem.2015.04.007, 2015.

1110 Gerringa, L. J. A., Slagter, H. A., Bown, J., van Haren, H., Laan, P., de Baar, H. J. W., and Rijkenberg, M. J. A.:  
1111 Dissolved Fe and Fe-binding organic ligands in the Mediterranean Sea – GEOTRACES G04, *Marine Chemistry*,  
1112 194, 100-113, 10.1016/j.marchem.2017.05.012, 2017.

1113 Gourain, A., Planquette, H., Cheize, M., Lemaitre, N., Menzel Barraqueta, J.-L., Shelley, R., Lherminier, P., and  
1114 Sarthou, G.: Inputs and processes affecting the distribution of particulate iron in the North Atlantic along the  
1115 GEOVIDE (GEOTRACES GA01) section, *Biogeosciences*, 16, 1563–1582, [https://doi.org/10.5194/bg-16-1563-](https://doi.org/10.5194/bg-16-1563-2019)  
1116 2019, 2019.

1117 Guerzoni, S., Chester, R., Dulac, F., Herut, B., Loye-Pilot, M.-D., Measures, C., Migon, C., Molinaroli, E., Moulin,  
1118 C., Rossini, P., Saydam, C., Soudine, A., and Ziveri, P.: The role of atmospheric deposition in the  
1119 biogeochemistry of the Mediterranean Sea, *Progress in Oceanography*, 44, 147-190,  
1120 [https://doi.org/10.1016/S0079-6611\(99\)00024-5](https://doi.org/10.1016/S0079-6611(99)00024-5), 1999.

1121 Guieu, C., Loye-Pilot, M. D., Benyahya, L., and Dufour, A.: Spatial variability of atmospheric fluxes of metals (Al,  
1122 Fe, Cd, Zn and Pb) and phosphorus over the whole Mediterranean from a one-year monitoring experiment:  
1123 Biogeochemical implications, *Marine Chemistry*, 120, 164-178, 10.1016/j.marchem.2009.02.004, 2010.

1124 Guieu, C., Aumont, O., Paytan, A., Bopp, L., Law, C. S., Mahowald, N., Achterberg, E. P., Marañón, E., Salihoglu,  
1125 B., Crise, A., Wagener, T., Herut, B., Desboeufs, K., Kanakidou, M., Olgun, N., Peters, F., Pulido-Villena, E.,  
1126 Tovar-Sanchez, A., and Völker, C.: The significance of the episodic nature of atmospheric deposition to Low  
1127 Nutrient Low Chlorophyll regions, *Global Biogeochemical Cycles*, 28, 1179-1198, 10.1002/2014gb004852,  
1128 2014.

1129 Harrison, W. G., Yngve Børshheim, K., Li, W. K. W., Maillet, G. L., Pepin, P., Sakshaug, E., Skogen, M. D., and  
1130 Yeats, P. A.: Phytoplankton production and growth regulation in the Subarctic North Atlantic: A comparative  
1131 study of the Labrador Sea-Labrador/Newfoundland shelves and Barents/Norwegian/Greenland seas and  
1132 shelves, *Progress in Oceanography*, 114, 26-45, 10.1016/j.pocean.2013.05.003, 2013.

1133 Hatta, M., Measures, C. I., Wu, J., Roshan, S., Fitzsimmons, J. N., Sedwick, P., and Morton, P.: An overview of  
1134 dissolved Fe and Mn distributions during the 2010-2011 US GEOTRACES north Atlantic cruises: GEOTRACES  
1135 GA03, *Deep-Sea Research Part II-Topical Studies in Oceanography*, 116, 117-129,  
1136 10.1016/j.dsr2.2014.07.005, 2015.

1137 Hawkings, J. R., Wadham, J. L., Tranter, M., Raiswell, R., Benning, L. G., Statham, P. J., Tedstone, A., Nienow,  
1138 P., Lee, K., and Telling, J.: Ice sheets as a significant source of highly reactive nanoparticulate iron to the  
1139 oceans, *Nature communications*, 5, 1-8, 10.1038/ncomms4929, 2014.

1140 Henson, S. A., Dunne, J. P., and Sarmiento, J. L.: Decadal variability in North Atlantic phytoplankton blooms,  
1141 *Journal of Geophysical Research*, 114, 10.1029/2008jc005139, 2009.

1142 Ho, T.-Y., Quigg, A., Finkel, Z. V., Milligan, A. J., Wyman, K., Falkowski, P. G., and Morel, F. M. M.: The elemental  
1143 composition of some marine phytoplankton, *Journal of Phycology*, 39, 1145-1159,  
1144 <https://doi.org/10.1111/j.0022-3646.2003.03-090.x>, 2003.

1145 Homoky, W. B., Hembury, D. J., Hepburn, L. E., Mills, R. A., Statham, P. J., Fones, G. R., and Palmer, M. R.: Iron  
1146 and manganese diagenesis in deep sea volcanogenic sediments and the origins of pore water colloids,  
1147 *Geochimica Et Cosmochimica Acta*, 75, 5032-5048, 10.1016/j.gca.2011.06.019, 2011.

1148 Homoky, W. B., John, S. G., Conway, T. M., and Mills, R. A.: Distinct iron isotopic signatures and supply from  
1149 marine sediment dissolution, *Nature Communications*, 4, 10.1038/ncomms3143, 2013.

1150 Humphreys, M. P., Griffiths, A. M., Achterberg, E. P., Holliday, N. P., Rérolle, V., Menzel Barraqueta, J. L., Couldrey,  
1151 M. P., Oliver, K. I., Hartman, S. E., and Esposito, M.: Multidecadal accumulation of anthropogenic and  
1152 remineralized dissolved inorganic carbon along the Extended Ellett Line in the northeast Atlantic Ocean, *Global  
1153 Biogeochemical Cycles*, 30, 293-310, doi: 10.1002/2015GB005246, 2016.

1154 Hunke, E. C., Notz, D., Turner, A. K., and Vancoppenolle, M.: The multiphase physics of sea ice: a review for model  
1155 developers, *The Cryosphere*, 5, 989-1009, 10.5194/tc-5-989-2011, 2011.

1156 Janssens, J., Meiners, K. M., Tison, J.-L., Dieckmann, G., Delille, B., and Lannuzel, D.: Incorporation of iron and  
1157 organic matter into young Antarctic sea ice during its initial growth stages, *Elementa: Science of the  
1158 Anthropocene*, 4, 000123, 10.12952/journal.elementa.000123, 2016.

1159 Jickells, T., and Moore, C. M.: The importance of atmospheric deposition for ocean productivity, *Annual Review of  
1160 Ecology, Evolution, and Systematics*, 46, 481-501, 10.1146/annurev-ecolsys-112414-054118, 2015.

1161 Jickells, T. D., An, Z. C., Andersen, K. K., Baker, A. R., Bergametti, G., Brooks, N., Cao, J. J., Boyd, P. W., Duce,  
1162 R. A., Hunter, K. A., Kawahata, H., Kubilay, N., laRoche, J., Liss, P. S., Mahowald, N., Prospero, J. M., Ridgwell,  
1163 A. J., Tegen, I., and Torres, R.: Global iron connections between desert dust, ocean biogeochemistry, and  
1164 climate, *Science*, 308, 67-71, DOI: 10.1126/science.1105959, 2005.

1165 Jones, E. P., Anderson, L. G., and Swift, J. H.: Distribution of Atlantic and Pacific waters in the upper Arctic Ocean:  
1166 Implications for circulation, *Geophysical Research Letters*, 25, 765-768, [https://doi-  
1167 org.inee.bib.cnrs.fr/10.1029/98GL00464](https://doi-org.inee.bib.cnrs.fr/10.1029/98GL00464), 1998.

1168 Kan, C. C., Chen, W. H., Wan, M. W., Phatai, P., Wittayakun, J., and Li, K. F.: The preliminary study of iron and  
1169 manganese removal from groundwater by NaOCl oxidation and MF filtration, *Sustain. Environ. Res.*, 22, 25-30,  
1170 2012.

1171 Kanzow, T. and Zenk, W.: Structure and transport of the Iceland Scotland Overflow plume along the Reykjanes  
1172 Ridge in the Iceland Basin, *Deep Sea Research Part I: Oceanographic Research Papers*, 86, 82–93,  
1173 doi:10.1016/j.dsr.2013.11.003, 2014

- 1174 Kara, A. B., Rochford, P. A., and Hurlburt, H. E.: An optimal definition for ocean mixed layer depth, *Journal of*  
 1175 *Geophysical Research*, 105, 16,803-816,821, 10.1029/2000JC900072, 2000.
- 1176 Käse, R. H., Girton, J. B. and Sanford, T. B.: Structure and variability of the Denmark Strait Overflow: Model and  
 1177 observations, *Journal of Geophysical Research: Oceans*, 108(C6), doi:10.1029/2002JC001548, 2003.
- 1178 Kissel, C., Laj, C., Mulder, T., Wandres, C., and Cremer, M.: The magnetic fraction: A tracer of deep water  
 1179 circulation in the North Atlantic, *Earth and Planetary Science Letters*, 288, 444-454, 10.1016/j.epsl.2009.10.005,  
 1180 2009.
- 1181 Klunder, M. B., Bauch, D., Laan, P., de Baar, H. J. W., van Heuven, S. M. A. C., and Ober, S.: Dissolved iron in the  
 1182 Arctic shelf seas and surface waters of the Central Arctic Ocean: impact of Arctic river water and ice-melt,  
 1183 *Journal of Geophysical Research*, 117, 1-18, <https://doi-org.inee.bib.cnrs.fr/10.1029/2011JC007133>, 2012.
- 1184 Lackschewitz, K. S., Ender, R., Gehrke, B., Wallrabe-Adams, H.-J., and Thiede, J.: Evidence for topography- and  
 1185 current-controlled deposition on the reykjanes Ridge between 59°N and 60°N, *Deep-Sea Research I*, 43, 1683-  
 1186 1711, [https://doi.org/10.1016/S0967-0637\(96\)00090-8](https://doi.org/10.1016/S0967-0637(96)00090-8), 1996.
- 1187 Laes, A., Blain, S., Laan, P., Achterberg, E. P., Sarthou, G., and de Baar, H. J. W.: Deep dissolved iron profiles in  
 1188 the eastern North Atlantic in relation to water masses, *Geophysical Research Letters*, 30,  
 1189 10.1029/2003gl017902, 2003.
- 1190 Lagerström, M. E., Field, M. P., Seguret, M., Fischer, L., Hann, S., and Sherrell, R. M.: Automated on-line flow-  
 1191 injection ICP-MS determination of trace metals (Mn, Fe, Co, Ni, Cu and Zn) in open ocean seawater: Application  
 1192 to the GEOTRACES program, *Marine Chemistry*, 155, 71-80, 10.1016/j.marchem.2013.06.001, 2013.
- 1193 Lambelet, M., van de Flierdt, T., Crocket, K., Rehkemper, M., Katharina, K., Coles, B., Rijkenberg, M. J. A.,  
 1194 Gerringa, L. J. A., de Baar, H. J. W., and Steinfeldt, R.: Neodymium isotopic composition and concentration in  
 1195 the western North Atlantic Ocean: Results from the GEOTRACES GA02 section, *Geochimica Et Cosmochimica*  
 1196 *Acta*, 177, 1-29, <https://doi.org/10.1016/j.gca.2015.12.019>, 2016.
- 1197 Le Roy, E., Sanial, V., Charette, M. A., van Beek, P., Lacan, F., Jacquet, S. H. M., Henderson, P. B., Souhaut, M.,  
 1198 García-Ibáñez, M. I., Jeandel, C., Pérez, F. F., and Sarthou, G.: The <sup>226</sup>Ra–Ba relationship in the North Atlantic  
 1199 during GEOTRACES-GA01, *Biogeosciences*, 15, 3027-3048, 10.5194/bg-15-3027-2018, 2018.
- 1200 Lemaitre, N., Planchon, F., Planquette, H., Dehairs, F., Fonseca-Batista, D., Roukaerts, A., Deman, F., Tang, Y.,  
 1201 Mariez, C., and Sarthou, G.: High variability of particulate organic carbon export along the North Atlantic  
 1202 GEOTRACES section GA01 as deduced from <sup>234</sup>Th fluxes, *Biogeosciences*, 15, 6417–6437,  
 1203 <https://doi.org/10.5194/bg-15-6417-2018>, 2018. .
- 1204 Lemaitre, N., Planquette, H., Planchon, F., Sarthou, G., Jacquet, S., García-Ibáñez, M. I., Gourain, A., Cheize, M.,  
 1205 Monin, L., André, L., Laha, P., Terry, H., and Dehairs, F.: Particulate barium tracing of significant mesopelagic  
 1206 carbon remineralisation in the North Atlantic, *Biogeosciences*, 15, 2289–2307, [https://doi.org/10.5194/bg-15-](https://doi.org/10.5194/bg-15-2289-2018)  
 1207 2289-2018, 2018.

1208 Lohan, M. C., and Bruland, K. W.: Elevated Fe(II) and Dissolved Fe in Hypoxic Shelf Waters off Oregon and  
1209 Washington: An Enhanced Source of Iron to Coastal Upwelling Regimes, *Environmental Science & Technology*,  
1210 42, 6462-6468, 10.1021/es800144j, 2008.

1211 Longhurst, A. R.: *Ecological geography of the Sea*, Second Edition ed., Elsevier Academic Press publications,  
1212 Burlington, 542 pp., 2007.

1213 Louanchi, F., and Najjar, R. G.: Annual cycles of nutrients and oxygen in the upper layers of the North Atlantic  
1214 Ocean, *Deep Sea Research Part II: Topical Studies in Oceanography*, 48, 2155-2171,  
1215 [https://doi.org/10.1016/S0967-0645\(00\)00185-5](https://doi.org/10.1016/S0967-0645(00)00185-5), 2001.

1216 Markus, T., Stroeve, J. C., and Miller, J.: Recent changes in Arctic sea ice melt onset, freezeup, and melt season  
1217 length, *Journal of Geophysical Research*, 114, 10.1029/2009jc005436, 2009.

1218 Marshall, J., and Schott, F.: Open-ocean convection: observations, theory, and models, *Reviews of Geophysics*,  
1219 37, 1-64, doi: 10.1029/98RG02739, 1999.

1220 Martin, J.-M., Elbaz-Poulichet, F., Guieu, C., Lo e-Pilot, M.-D., and Han, G.: River versus atmospheric input of  
1221 material to the Mediterranean Sea: an overview, *Marine Chemistry*, 28, 159-182, [https://doi.org/10.1016/0304-](https://doi.org/10.1016/0304-4203(89)90193-X)  
1222 [4203\(89\)90193-X](https://doi.org/10.1016/0304-4203(89)90193-X), 1989.

1223 Martin, J. D., and Fitzwater, S. E.: Iron deficiency limits phytoplankton growth in the north-east Pacific subarctic,  
1224 *Nature*, 331, 341-343, 1988.

1225 Martin, J. H., Fitzwater, S. E., and Gordon, R. M.: Iron deficiencies limits phytoplankton growth in Antarctic waters,  
1226 *Global Biogeochemical Cycles*, 4, 5-12, <https://doi-org.inee.bib.cnrs.fr/10.1029/GB004i001p00005>, 1990.

1227 Martin, J. H., Coale, K. H., Johnson, K. S., Fitzwater, S. E., Gordon, R. M., Tanner, S. J., Hunter, C. N., Elrod, V.  
1228 A., Nowicki, J. L., Coley, T. L., Barber, R. T., Lindley, S., Watson, A. J., Van Scoy, K., Law, C. S., Liddicoat, M.  
1229 I., Ling, R., Stanton, T., Stockel, J., Collins, C., Anderson, A., Bidigare, R., Ondrusek, M., Latasa, M., Millero, F.  
1230 J., Lee, K., Yao, W., Zhang, J. Z., Friederich, G., Sakamoto, C., Chavez, F., Buck, K., Kolber, Z., Greene, R.,  
1231 Falkowski, P., Chisholm, S. W., Hoge, F., Swift, R., Yungel, J., Turner, S., Nightingale, P., Hatton, A., Liss, P.,  
1232 and Tindale, N. W.: Testing the Iron Hypothesis in Ecosystems of the Equatorial Pacific Ocean, *Nature*, 371,  
1233 123-129, 10.1038/371123a0, 1994.

1234 Measures, C. I., Brown, M. T., Selph, K. E., Apprill, A., Zhou, M., Hatta, M., and Hiscock, W. T.: The influence of  
1235 shelf processes in delivering dissolved iron to the HNLC waters of the Drake Passage, Antarctica, *Deep Sea*  
1236 *Research Part II: Topical Studies in Oceanography*, 90, 77-88, 10.1016/j.dsr2.2012.11.004, 2013.

1237 Melling, H., and Moore, R. M.: Modification of halocline source waters during freezing on the Beaufort Sea shelf:  
1238 Evidence from oxygen isotopes and dissolved nutrients, *Continental Shelf Research*, 15, 89-113,  
1239 [https://doi.org/10.1016/0278-4343\(94\)P1814-R](https://doi.org/10.1016/0278-4343(94)P1814-R), 1995.

1240 Menzel Barraqueta, J.-L., Schlosser, C., Planquette, H., Gourain, A., Cheize, M., Boutorh, J., Shelley, R., Contreira  
1241 Pereira, L., Gledhill, M., Hopwood, M. J., Lacan, F., Lherminier, P., Sarthou, G., and Acherberg, E. P.:  
1242 Aluminium in the North Atlantic Ocean and the Labrador Sea (GEOTRACES GA01 section): roles of continental



1243 inputs and biogenic particle removal, *Biogeosciences*, 15, 5271–5286, [https://doi.org/10.5194/bg-15-5271-](https://doi.org/10.5194/bg-15-5271-2018)  
1244 2018, 2018. .

1245 Mercier, H., Lherminier, P., Sarafanov, A., Gaillard, F., Daniault, N., Desbruyères, D., Falina, A., Ferron, B.,  
1246 Gourcuff, C., Huck, T., and Thierry, V.: Variability of the meridional overturning circulation at the Greenland–  
1247 Portugal OVIDE section from 1993 to 2010, *Progress in Oceanography*, 132, 250-261,  
1248 10.1016/j.pocean.2013.11.001, 2015.

1249 Mil-Homens, M., Branco, V., Lopes, C., Vale, C., Abrantes, F., Boer, W., and Vicente, M.: Using factor analysis to  
1250 characterise historical trends of trace metal contamination in a sediment core from the Tagus Prodelta, Portugal,  
1251 *Water, Air, and Soil Pollution*, 197, 277-287, <https://doi.org/10.1007/s11270-008-9810-0>, 2009.

1252 Moore, C. M., Mills, M. M., Langlois, R., Milne, A., Achterberg, E. P., La Roche, J., and Geider, R. J.: Relative  
1253 influence of nitrogen and phosphorus availability on phytoplankton physiology and productivity in the oligotrophic  
1254 sub-tropical North Atlantic Ocean, *Limnology and Oceanography*, 53, 291-205, [https://doi-](https://doi-org.inee.bib.cnrs.fr/10.4319/lo.2008.53.1.0291)  
1255 [org.inee.bib.cnrs.fr/10.4319/lo.2008.53.1.0291](https://doi-org.inee.bib.cnrs.fr/10.4319/lo.2008.53.1.0291), 2008.

1256 Moore, C. M., Mills, M. M., Arrigo, K. R., Berman-Frank, I., Bopp, L., Boyd, P. W., Galbraith, E. D., Geider, R. J.,  
1257 Guieu, C., Jaccard, S. L., Jickells, T. D., La Roche, J., Lenton, T. M., Mahowald, N. M., Marañón, E., Marinov,  
1258 I., Moore, J. K., Nakatsuka, T., Oschlies, A., Saito, M. A., Thingstad, T. F., Tsuda, A., and Ulloa, O.: Processes  
1259 and patterns of oceanic nutrient limitation, *Nature Geoscience*, 6, 701-710, 10.1038/ngeo1765, 2013.

1260 Moore, G. W. K.: Gale force winds over the Irminger Sea to the east of Cape Farewell, Greenland, *Geophysical*  
1261 *Research Letters*, 30, 17, 10.1029/2003gl018012, 2003.

1262 Nielsdóttir, M. C., Moore, C. M., Sanders, R., Hinz, D. J., and Achterberg, E. P.: Iron limitation of the postbloom  
1263 phytoplankton communities in the Iceland Basin, *Global Biogeochemical Cycles*, GB3001,  
1264 doi:10.1029/2008GB003410, 2009.

1265 Olafsson, J., Thors, K., and Cann, J. R.: A sudden cruise off Iceland, *RIDGE Events*, 2, 35-28, 1991.

1266 Oschlies, A.: Nutrient supply to the surface waters of the North Atlantic: A model study, *Journal of Geophysical*  
1267 *Research*, 107, 10.1029/2000jc000275, 2002.

1268 Painter, S. C., Henson, S. A., Forryan, A., Steigenberger, S., Klar, J., Stinchcombe, M. C., Rogan, N., Baker, A. R.,  
1269 Achterberg, E. P., and Moore, C. M.: An assessment of the vertical diffusive flux of iron and other nutrients to  
1270 the surface waters of the subpolar North Atlantic Ocean, *Biogeosciences*, 11, 2113-2130, 10.5194/bg-11-2113-  
1271 2014, 2014.

1272 Palmer, M. R., Ludford, E. M., German, C. R., and Lilley, M. D.: Dissolved methane and hydrogen in the Steinahóll  
1273 hydrothermal plume, 63°N, Reykjanes Ridge, in: *Hydrothermal Vents and Processes*, edited by: Parson, L. M.,  
1274 Walker, C. L., and Dixon, D. R., Special Publications, Geological Society, London, 111-120, 1995.

1275 Parekh, P., Follows, M. J., and Boyle, E. A.: Decoupling of iron and phosphate in the global ocean, *Global*  
1276 *Biogeochemical Cycle*, 19, GB2020, <https://doi-org.inee.bib.cnrs.fr/10.1029/2004GB002280>, 2005.

1277 Parra, M., Delmont, P., Ferragne, A., Latouche, C., Pons, J. C., and Puechmaille, C.: Origin and evolution of  
1278 smectites in recent marine sediments of the NE Atlantic, *Clay Minerals*, 20, 335-346,  
1279 <https://doi.org/10.1180/claymin.1985.020.3.06>, 1985.

1280 Pérez, F. F., Mercier, H., Vázquez-Rodríguez, M., Lherminier, P., Velo, A., Pardo, P. C., Rosón, G., and Ríos, A.  
1281 F.: Atlantic Ocean CO<sub>2</sub> uptake reduced by weakening of the meridional overturning circulation, *Nature*  
1282 *Geoscience*, 6, 146-152, 10.1038/ngeo1680, 2013.

1283 Pérez, F. F., Treguer, P., Branellec, P., García-Ibáñez, M. I., Lherminier, P., and Sarthou, G.: The 2014 Greenland-  
1284 Portugal GEOVIDE bottle data (GO-SHIP A25 and GEOTRACES GA01). SEANOE (Ed.), 2018.

1285 Petrich, C., and Eicken, H.: Growth, structure and properties of sea ice, in: *Sea Ice*. 2nd ed., edited by: Thomas, D.  
1286 N., and Dieckmann, G. S., Wiley-Blackwell, Oxford, U.K., 23-77, 2010.

1287 Pickart, R. S., Straneo, F., and Moore, G. W. K.: Is Labrador Sea Water formed in the Irminger basin?, *Deep Sea*  
1288 *Research Part I*, 50, 23-52, [https://doi.org/10.1016/S0967-0637\(02\)00134-6](https://doi.org/10.1016/S0967-0637(02)00134-6), 2003.

1289 Piron, A., Thierry, V., Mercier, H., and Caniaux, G.: Argo float observations of basin-scale deep convection in the  
1290 Irminger sea during winter 2011–2012, *Deep Sea Research Part I: Oceanographic Research Papers*, 109, 76-  
1291 90, 10.1016/j.dsr.2015.12.012, 2016.

1292 Radic, A., Lacan, F., and Murray, J. W.: Iron isotopes in the seawater of the equatorial Pacific Ocean: New  
1293 constraints for the oceanic iron cycle, *Earth and Planetary Science Letters*, 306, 1-10,  
1294 10.1016/j.epsl.2011.03.015, 2011.

1295 Ras, J., Claustre, H., and Uitz, J.: Spatial variability of phytoplankton pigment distribution in the Subtropical South  
1296 Pacific Ocean: comparison between *in situ* and predicted data, *Biogeosciences*, 5, 353-369,  
1297 <https://doi.org/10.5194/bg-5-353-2008>, 2008.

1298 Riebesell, U., Schloss, I., and Smetacek, V.: Aggregation of algae released from melting sea ice: implications for  
1299 seeding and sedimentation, *Polar Biology*, 11, 239-248, <https://doi.org/10.1007/BF00238457>, 1991.

1300 Rijkenberg, M. J., Middag, R., Laan, P., Gerringa, L. J., van Aken, H. M., Schoemann, V., de Jong, J. T., and de  
1301 Baar, H. J.: The distribution of dissolved iron in the West Atlantic Ocean, *PLoS One*, 9, e101323,  
1302 10.1371/journal.pone.0101323, 2014.

1303 Sabine, C. L., Feely, R. A., Gruber, N., Key, R. M., Lee, K., Bullister, J. L., Wanninkhof, R., Wong, C. S., Wallace,  
1304 D. W. R., Tilbrook, B., Millero, F. J., Peng, T.-H., Kozyr, A., Ono, T., and Rios, A. F.: The Oceanic sink for  
1305 anthropogenic CO<sub>2</sub>, *Science*, 305, 367-371, 10.1126/science.1097403, 2004.

1306 Sanders, R., Brown, L., Henson, S., and Lucas, M.: New production in the Irminger Basin during 2002, *Journal of*  
1307 *Marine Systems*, 55, 291-310, [http:// dx.doi.org/10.1016/j.jmarsys.2004.09.002](http://dx.doi.org/10.1016/j.jmarsys.2004.09.002), 2005.

1308 Santos-Echeandia, J., Vale, C., Caetano, M., Pereira, P., and Prego, R.: Effect of tidal flooding on metal distribution  
1309 in pore waters of marsh sediments and its transport to water column (Tagus estuary, Portugal), *Mar Environ*  
1310 *Res*, 70, 358-367, 10.1016/j.marenvres.2010.07.003, 2010.

1311 Sarthou, G., and Jeandel, C.: Seasonal variations of iron concentrations in the Ligurian Sea and iron budget in the  
1312 Western Mediterranean Sea, *Marine Chemistry*, 74, 115-129, 10.1016/s0304-4203(00)00119-5, 2001.

1313 Sarthou, G., Baker, A. R., Kramer, J., Laan, P., Laës, A., Ussher, S., Achterberg, E. P., de Baar, H. J. W.,  
1314 Timmermans, K. R., and Blain, S.: Influence of atmospheric inputs on the iron distribution in the subtropical  
1315 North-East Atlantic Ocean, *Marine Chemistry*, 104, 186-202, 10.1016/j.marchem.2006.11.004, 2007.

1316

1317 Sarthou, G., Laan, P., Ussher, S., Kramer, J., Timmermans, K. R. and Blain, S.: Influence of high atmospheric  
1318 inputs on the iron distribution in the water column of the North Atlantic Ocean., 2003.

1319 Sarthou, G., Lherminier, P., Achterberg, E. P., Alonso-Pérez, F., Bucciarelli, E., Boutorh, J., Bouvier, V., Boyle, E.  
1320 A., Branellec, P., Carracedo, L. I., Casacuberta, N., Castrillejo, M., Cheize, M., Contreira Pereira, L., Cossa, D.,  
1321 Daniault, N., De Saint-Léger, E., Dehairs, F., Deng, F., Desprez de Gésincourt, F., Devesa, J., Foliot, L.,  
1322 Fonseca-Batista, D., Gallinari, M., García-Ibáñez, M. I., Gourain, A., Grossteffan, E., Hamon, M., Heimbürger,  
1323 L. E., Henderson, G. M., Jeandel, C., Kermabon, C., Lacan, F., Le Bot, P., Le Goff, M., Le Roy, E., Lefèbvre,  
1324 A., Leizour, S., Lemaitre, N., Masqué, P., Ménage, O., Menzel Barraqueta, J.-L., Mercier, H., Perault, F., Pérez,  
1325 F. F., Planquette, H. F., Planchon, F., Roukaerts, A., Sanial, V., Sauzède, R., Schmechtig, C., Shelley, R. U.,  
1326 Stewart, G., Sutton, J. N., Tang, Y., Tisnérat-Laborde, N., Tonnard, M., Tréguer, P., van Beek, P., Zurbrick, C.  
1327 M., and Zunino, P.: Introduction to the French GEOTRACES North Atlantic Transect (GA01): GEOVIDE cruise,  
1328 *Biogeosciences*, 15, 7097–7109, <https://doi.org/10.5194/bg-15-7097-2018>, 2018.

1329

1330 Sarthou, G., Vincent, D., Christaki, U., Obernosterer, I., Timmermans, K. R., and Brussaard, C. P. D.: The fate of  
1331 biogenic iron during a phytoplankton bloom induced by natural fertilisation: Impact of copepod grazing, *Deep  
1332 Sea Research Part II: Topical Studies in Oceanography*, 55, 734-751, 10.1016/j.dsr2.2007.12.033, 2008.

1333 Ocean Data View, <https://odv.awi.de> ODV4, version 4.7.6 (23 March 2016), access: 6 April, 2016.

1334 Schmidt, S. and Reys, J.-L.: Radium as internal tracer of Mediterranean Outflow Water, *Journal of Geophysical  
1335 Research*, 101, 3589–3596, 1996.

1336 Schroth, A. W., Crusius, J., Hoyer, I., and Campbell, R.: Estuarine removal of glacial iron and implications for iron  
1337 fluxes to the ocean, *Geophysical Research Letters*, 41, 3951-3958, 10.1002/2014GL060199, 2014.

1338 Shelley, R. U., Morton, P. L., and Landing, W. M.: Elemental ratios and enrichment factors in aerosols from the US-  
1339 GEOTRACES North Atlantic transects, *Deep Sea Research*, 116, 262-272,  
1340 <https://doi.org/10.1016/j.dsr2.2014.12.005>, 2015.

1341 Shelley, R. U., Roca-Martí, M., Castrillejo, M., Sanial, V., Masqué, P., Landing, W. M., van Beek, P., Planquette,  
1342 H., and Sarthou, G.: Quantification of trace element atmospheric deposition fluxes to the Atlantic Ocean (>40°N;  
1343 GEOVIDE, GEOTRACES GA01) during spring 2014, *Deep Sea Research Part I: Oceanographic Research  
1344 Papers*, 119, 34-49, 10.1016/j.dsr.2016.11.010, 2017.

1345 Shelley, R. U., Landing, W. M., Ussher, S. J., Planquette, H., and Sarthou, G.: Regional trends in the fractional  
1346 solubility of Fe and other metals from North Atlantic aerosols (GEOTRACES cruises GA01 and GA03) following  
1347 a two-stage leach, *Biogeosciences*, 15, 2271–2288, <https://doi.org/10.5194/bg-15-2271-2018>, 2018.

1348 Shor, A., Lonsdale, P., Hollister, D., and Spencer, D.: Charlie-Gibbs fracture zone: bottom-water transport and its  
1349 geological effects, *Deep Sea Research*, 27A, 325-345, [https://doi.org/10.1016/0198-0149\(80\)90030-8](https://doi.org/10.1016/0198-0149(80)90030-8), 1980.

1350 Sinha, M. C., Navin, D. A., MacGregor, L. M., Constable, S., Peirce, C., White, A., Heinson, G., and Inglis, M. A.:  
1351 Evidence for accumulated melt beneath the slow-spreading Mid-Atlantic Ridge, *Philosophical Transactions of  
1352 the Royal Society A*, 355, 233-253, <https://doi.org/10.1098/rsta.1997.0008>, 1997.

1353 Slagter, H. A., Reader, H. E., Rijkenberg, M. J. A., Rutgers van der Loeff, M., de Baar, H. J. W., and Gerringa, L. J.  
1354 A.: Organic Fe speciation in the Eurasian Basins of the Arctic Ocean and its relation to terrestrial DOM, *Marine  
1355 Chemistry*, 197, 11-25, [10.1016/j.marchem.2017.10.005](https://doi.org/10.1016/j.marchem.2017.10.005), 2017.

1356 Smallwood, J. R., and White, R. S.: Crustal accretion at the Reykjanes Ridge, 61°-62°N, *Journal of Geophysical  
1357 Research: Solid Earth*, 103, 5185-5201, [10.1029/97jb03387](https://doi.org/10.1029/97jb03387), 1998.

1358 Statham, P. J., Skidmore, M., and Tranter, M.: Inputs of glacially derived dissolved and colloidal iron to the coastal  
1359 ocean and implications for primary productivity, *Global Biogeochemical Cycles*, 22, 1-11,  
1360 [10.1029/2007GB003106](https://doi.org/10.1029/2007GB003106), 2008.

1361 Sunda, W. G., and Huntsman, S. A.: Iron uptake and growth limitation in oceanic and coastal phytoplankton, *Marine  
1362 Chemistry*, 50, 189-206, [10.1016/0304-4203\(95\)00035-p](https://doi.org/10.1016/0304-4203(95)00035-p), 1995.

1363 Sutherland, D. A., Pickart, R. S., Peter Jones, E., Azetsu-Scott, K., Jane Eert, A., and Ólafsson, J.: Freshwater  
1364 composition of the waters off southeast Greenland and their link to the Arctic Ocean, *Journal of Geophysical  
1365 Research*, 114, [10.1029/2008jc004808](https://doi.org/10.1029/2008jc004808), 2009.

1366 Tagliabue, A., Aumont, O., DeAth, R., Dunne, J. P., Dutkiewicz, S., Galbraith, E., Misumi, K., Moore, J. K., Ridgwell,  
1367 A., Sherman, E., Stock, C., Vichi, M., Völker, C. and Yool, A.: How well do global ocean biogeochemistry models  
1368 simulate dissolved iron distributions?, *Global Biogeochemical Cycles*, 30(2), 149–174,  
1369 [doi:10.1002/2015GB005289](https://doi.org/10.1002/2015GB005289), 2016.

1370 Tanhua, T., Olsson, K. A., and Jeansson, E.: Formation of Denmark Strait overflow water and its hydro-chemical  
1371 composition, *Journal of Marine Systems*, 57, 264-288, [10.1016/j.jmarsys.2005.05.003](https://doi.org/10.1016/j.jmarsys.2005.05.003), 2005.

1372 Teng, Z., Huang, J. Y., Fujito, K., and Takizawa, S.: Manganese removal by hollow fiber micro-filter. Membrane  
1373 separation for drinking water, *European Conference on Desalination and the Environment*, Amsterdam, 28  
1374 May, 2001.

1375 Thuróczy, C. E., Gerringa, L. J. A., Klunder, M. B., Middag, R., Laan, P., Timmermans, K. R., and de Baar, H. J.  
1376 W.: Speciation of Fe in the Eastern North Atlantic Ocean, *Deep Sea Research Part I: Oceanographic Research  
1377 Papers*, 57, 1444-1453, [10.1016/j.dsr.2010.08.004](https://doi.org/10.1016/j.dsr.2010.08.004), 2010.

1378 Tonnard, M., Donval, A., Lampert, L., Tréguer, P., Bowie, A. R., van der Merwe, P., planquette, H., Claustre, H.,  
1379 Dimier, C., Ras, J., and Sarthou, G.: Phytoplankton assemblages in the North Atlantic Ocean and in the

1380 Labrador Sea along the GEOVIDE section (GEOTRACES section GA01) determined by CHEMTAX analysis  
1381 from HPLC pigment data, *Biogeosciences*, in prep.

1382 Tovar-Sanchez, A., Duarte, C. M., Alonso, J. C., Lacorte, S., Tauler, R., and Galban-Malagon, C.: Impacts of metals  
1383 and nutrients released from melting multiyear Arctic sea ice, *Journal of Geophysical Research-Oceans*, 115,  
1384 10.1029/2009jc005685, 2010.

1385 Tréguer, P. J., and De La Rocha, C. L.: The world ocean silica cycle, *Ann Rev Mar Sci*, 5, 477-501,  
1386 10.1146/annurev-marine-121211-172346, 2013.

1387 Twining, B. S., Baines, S. B., Fisher, N. S., and Landry, M. R.: Cellular iron contents of plankton during the Southern  
1388 Ocean Iron Experiment (SOFeX), *Deep Sea Research Part I: Oceanographic Research Papers*, 51, 1827-1850,  
1389 10.1016/j.dsr.2004.08.007, 2004.

1390 Van Beusekom, J. E. E.: Distribution of aluminium in surface waters of the North Sea: influence of suspended  
1391 matter., in: *Biogeochemistry and Distribution of Suspended Matter in the North Sea and Implications to fisheries*  
1392 *Biology*, edited by: Kempe, S., *Mitteilungen aus dem Geologisch-Paläontologischen Institut der Universität*  
1393 *Hamburg*, SCOPE/UNEP Sonderband, 117-136, 1988.

1394 von Appen, W.-J., Koszalka, I. M., Pickart, R. S., Haine, T. W. N., Mastropole, D., Magaldi, M. G., Valdimarsson,  
1395 H., Girtton, J., Jochumsen, K., and Krahnmann, G.: The East Greenland Spill Jet as an important component of  
1396 the Atlantic Meridional Overturning Circulation, *Deep Sea Research Part I: Oceanographic Research Papers*,  
1397 92, 75-84, 10.1016/j.dsr.2014.06.002, 2014.

1398 Wadhams, P.: *Ice in the Ocean*, Gordon and Breach Science Publishers, London, UK, 2000.

1399 Wagener, T., Guieu, C., and Leblond, N.: Effects of dust deposition on iron cycle in the surface Mediterranean Sea:  
1400 results from a mesocosm seeding experiment, *Biogeosciences*, 7, 3769–3781, [https://doi.org/10.5194/bg-7-](https://doi.org/10.5194/bg-7-3769-2010)  
1401 [3769-2010](https://doi.org/10.5194/bg-7-3769-2010), 2010. .

1402 Woodgate, R. A., and Aagaard, K.: Revising the Bering Strait freshwater flux into the Arctic Ocean, *Geophysical*  
1403 *Research Letters*, 32, 10.1029/2004GL021747., 2005.

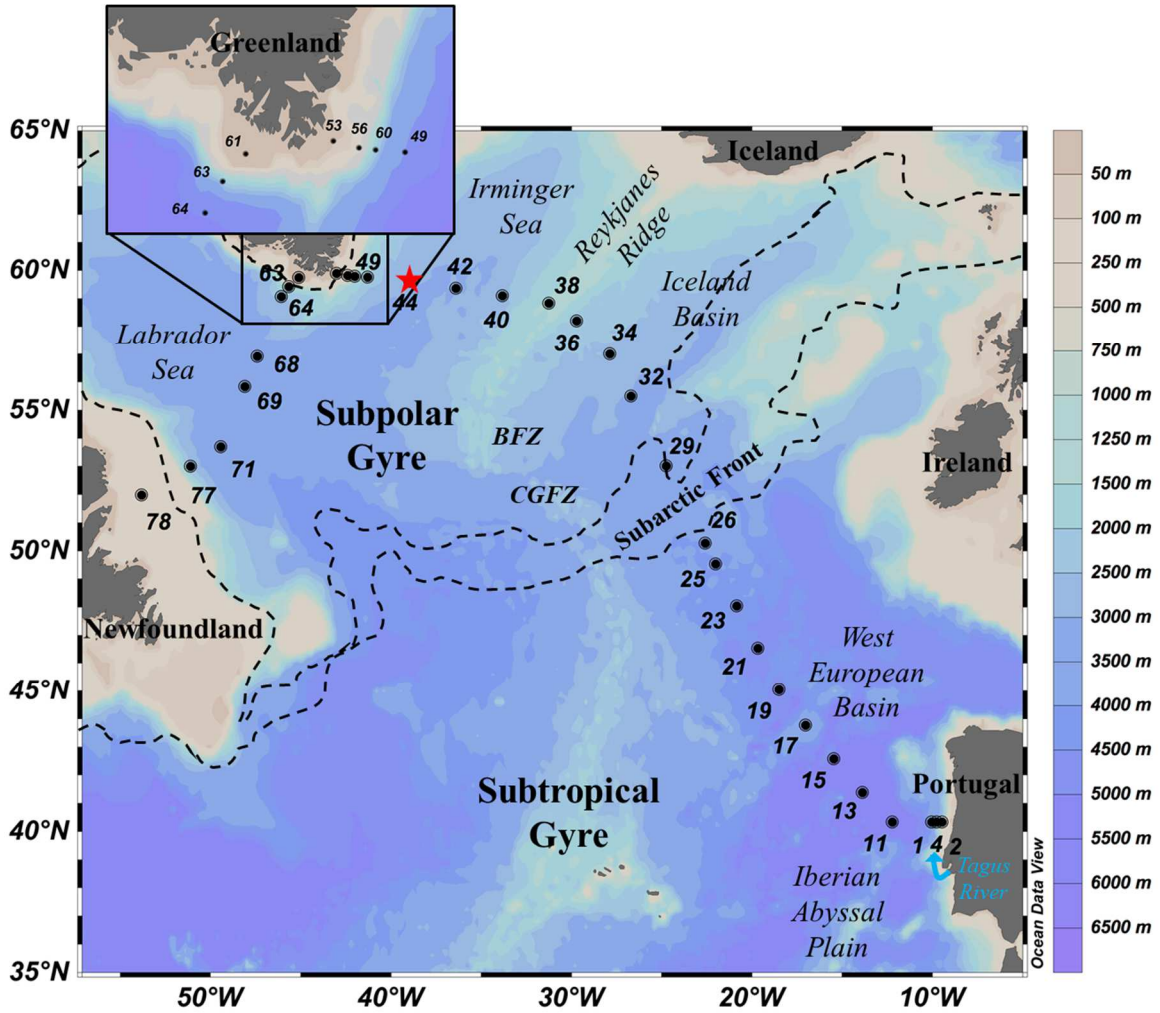
1404 Wuttig, K., Wagener, T., Bressac, M., Dammshäuser, A., Streu, P., Guieu, C., and Croot, P. L.: Impacts of dust  
1405 deposition on dissolved trace metal concentrations (Mn, Al and Fe) during a mesocosm experiment,  
1406 *Biogeosciences*, 10, 2583-2600, 10.5194/bg-10-2583-2013, 2013.

1407 Yashayaev, I., Bersch, M. and Aken, H. M. van: Spreading of the Labrador Sea Water to the Irminger and Iceland  
1408 basins, *Geophysical Research Letters*, 34(10), doi:10.1029/2006GL028999, 2007.

1409 Zou, S., Lozier, S., Zenk, W., Bower, A., and Johns, W.: Observed and modeled pathways of the Iceland Scotland  
1410 Overflow Water in the eastern North Atlantic, *Progress in Oceanography*, 159, 211-222,  
1411 10.1016/j.pocean.2017.10.003, 2017.

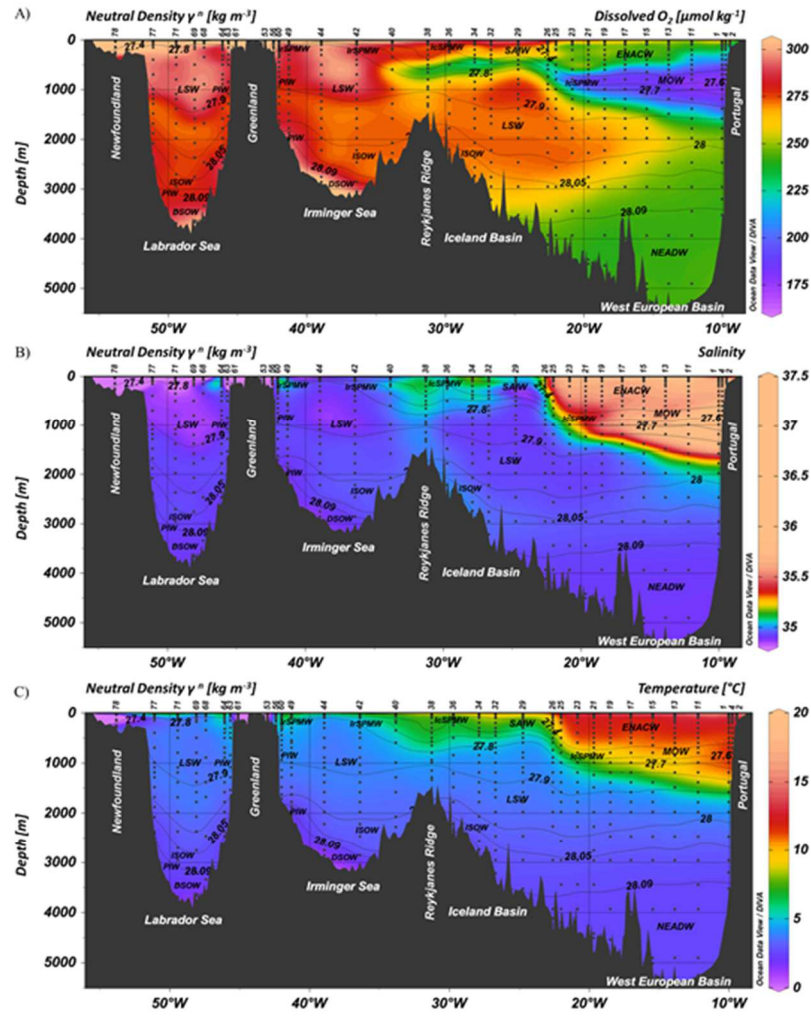
1412 Zunino, P., Lherminier, P., Mercier, H., Daniault, N., García-Ibáñez, M. I., and Pérez, F. F.: The GEOVIDE cruise  
1413 in May–June 2014 reveals an intense Meridional Overturning Circulation over a cold and fresh subpolar North  
1414 Atlantic, *Biogeosciences*, 14, 5323–5342, <https://doi.org/10.5194/bg-14-5323-2017>, 2017.

1415 Figure 1: Map of the GEOTRACES GA01 voyage plotted on bathymetry as well as the major topographical  
 1416 features and main basins. Crossover station with GEOTRACES voyage (GA03) is shown as a red star.  
 1417 (Ocean Data View (ODV) software, version 4.7.6, R. Schlitzer, <http://odv.awi.de>, 2016). BFZ: Bight Fracture  
 1418 Zone, CGFZ: Charlie-Gibbs Fracture Zone.  
 1419  
 1420



1421  
 1422

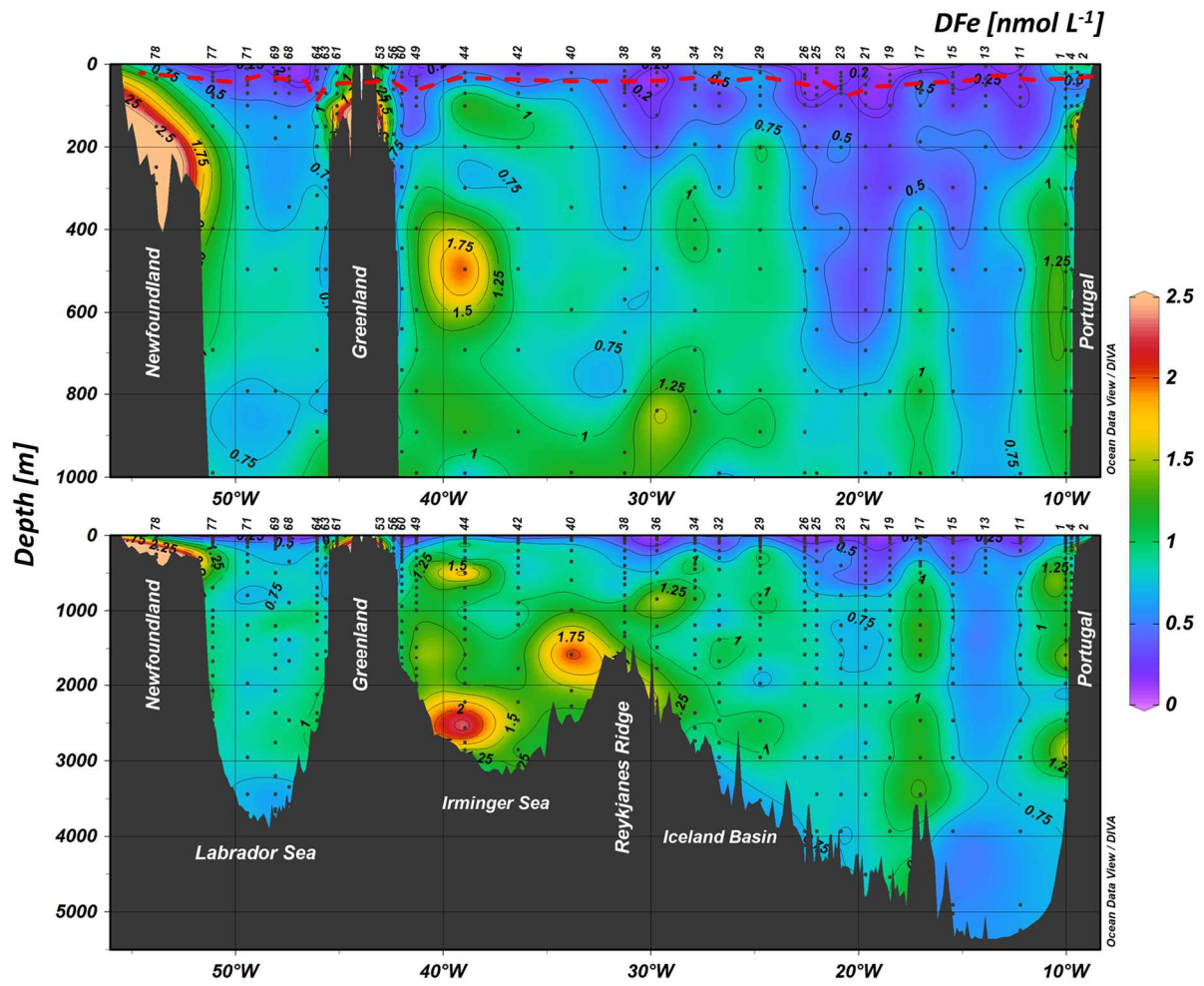
1423 Figure 2: Parameters measured from the regular CTD cast represented as a function of depth for GA01  
 1424 section for (A) Dissolved Oxygen ( $O_2$ ,  $\mu\text{mol kg}^{-1}$ ), (B) Salinity and (C) Temperature ( $^{\circ}\text{C}$ ). The contour lines  
 1425 represent isopycnals (neutral density,  $\gamma^n$ , in units of  $\text{kg m}^{-3}$ ).



Surface water masses		Overflow Deep water masses	
ENACW	East North Atlantic Central Water	NEADW	North East Atlantic Deep Water
IcSPMW	Iceland SubPolar Mode Water	PIW	Polar Intermediate Water
IrSPMW	Irminger SubPolar Mode Water	ISOW	Iceland-Scotland Overflow Water
SAIW	Subarctic Intermediate Water	DSOW	Denmark Strait Overflow Water
<b>Intermediate water masses</b>			
MOW	Mediterranean Outflow Water		
LSW	Labrador Sea Water		

1426  
 1427

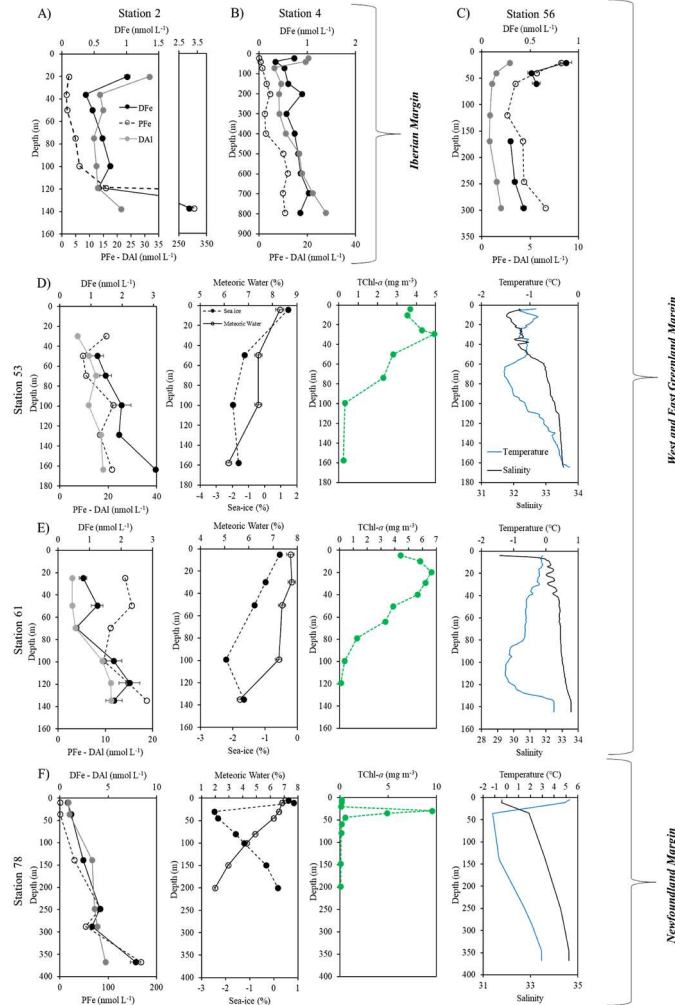
1428 Figure 3: Contour plot of the distribution of dissolved iron (DFe) concentrations in  $\text{nmol L}^{-1}$  along the GA01  
 1429 voyage transect: upper 1000 m (top) and full depth range (bottom). The red dashed line indicates the depth  
 1430 of the Surface Mixed Layer (SML). Small black dots represent collected water samples at each sampling  
 1431 station. (Ocean Data View (ODV) software, version 4.7.6, R. Schlitzer, <http://odv.awi.de>, 2016).



1432  
 1433  
 1434  
 1435  
 1436

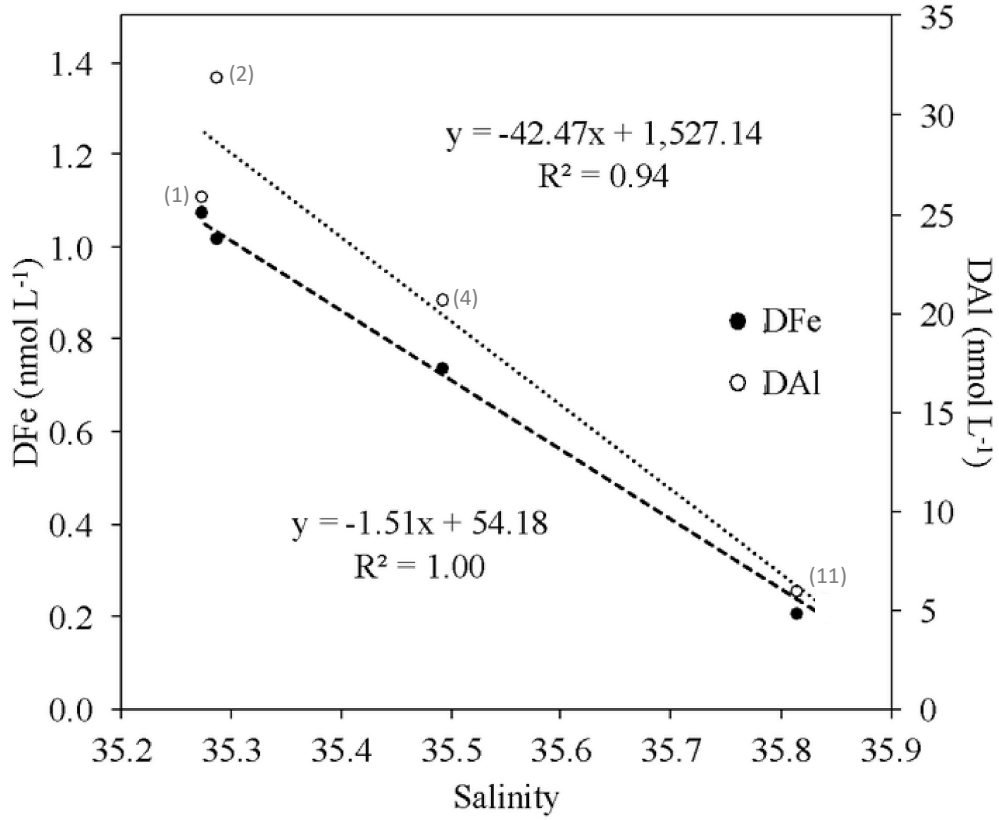


1437 Figure 4: Vertical profiles of dissolved iron (DFe, black dots, solid line), particulate iron (PFe, black open  
 1438 dots, dashed line, Gourain et al., 2019) and dissolved aluminium (DAI, grey dots, Menzel Barraqueta et al.,  
 1439 2018) at Stations 2 (A), and 4 (B) located above the Iberian shelf, Station 56 (C), Stations 53 (D) 53 and  
 1440 Station 61 (E) located above the Greenland shelf and Station 78 (F) located above the Newfoundland shelf.  
 1441 Note that for stations 53, 61 and 78, plots of the percentage of meteoric water (open dots) and sea-ice  
 1442 melting (black dots and dashed line) (Benetti et al., see text for details), Total Chlorophyll-a (TChl-a, green),  
 1443 temperature (blue) and salinity (black) are also displayed as a function of depth.



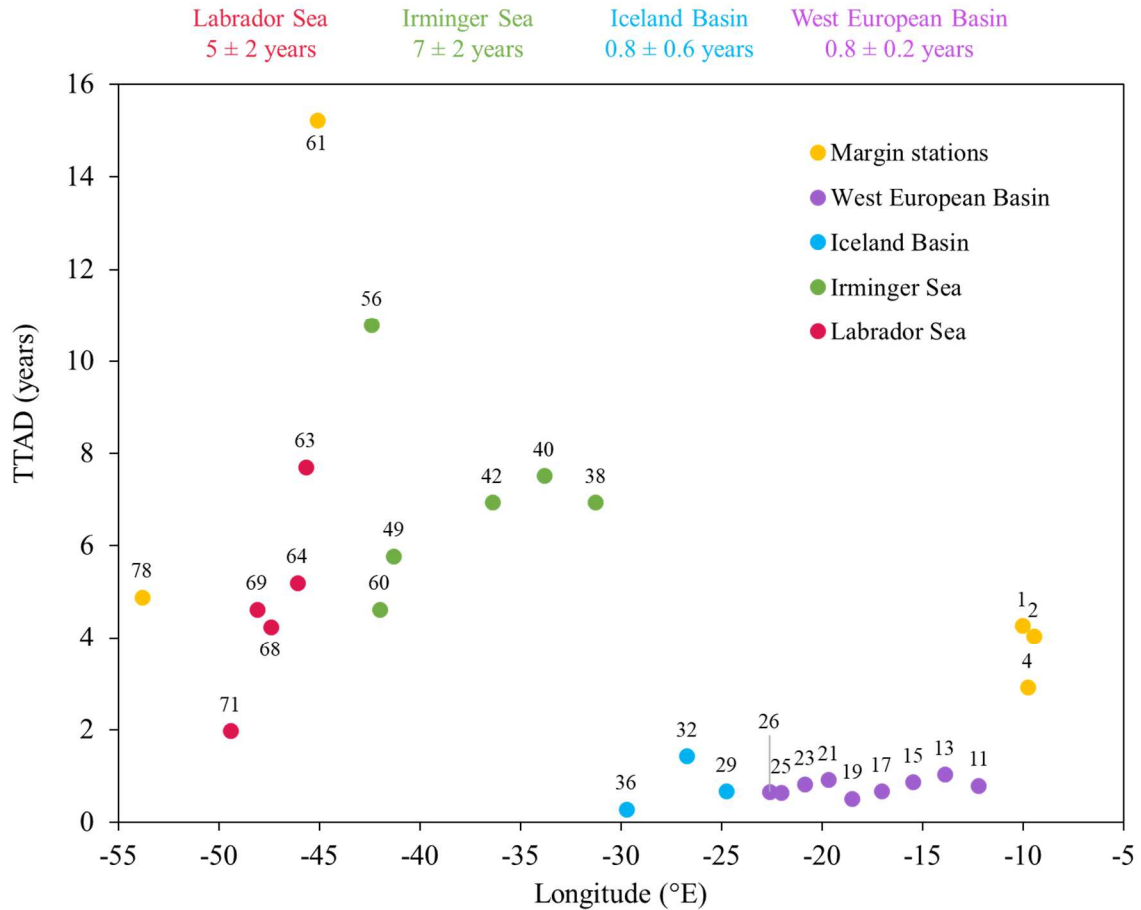
1444  
 1445  
 1446

1447 **Figure 5: Plot of dissolved iron (DFe, black circles) and dissolved aluminium (DAI, white circles, Menzel**  
1448 **Barraqueta et al., 2018) at ~ 20 m, along the salinity gradient between stations 1, 2, 4, and 11 with linear**  
1449 **regression equations. Numbers close to sample points representing station numbers.**  
1450



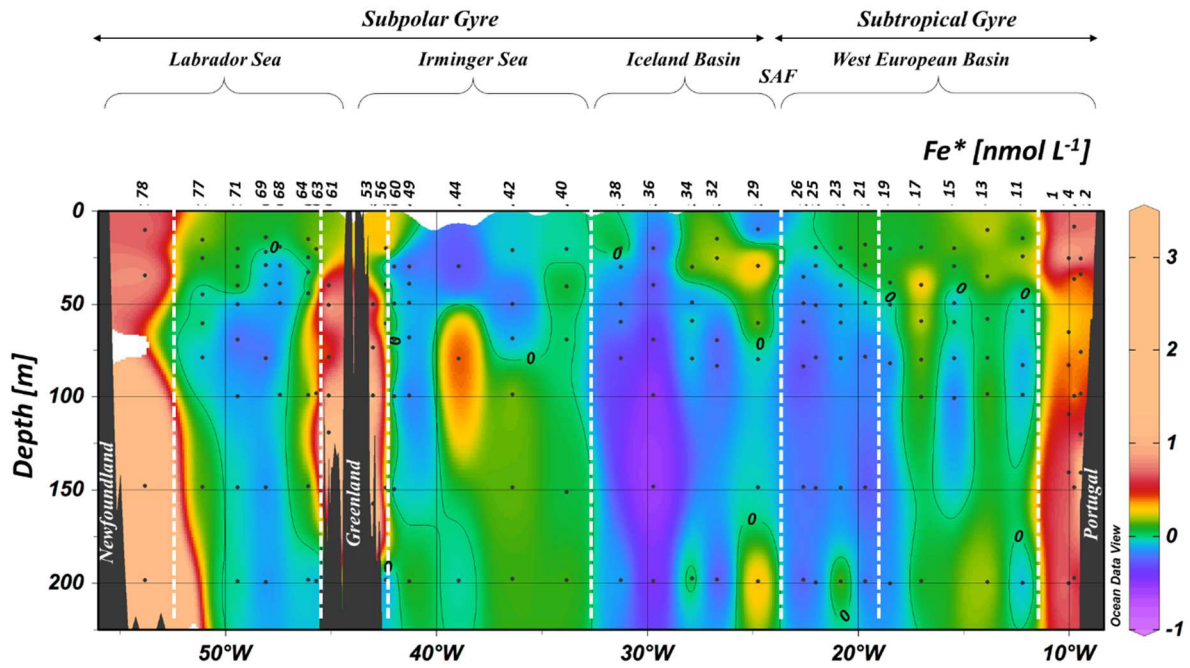
1451  
1452  
1453

1454 **Figure 6: Plot of dissolved Fe (DFe) Turnover Times relative to Atmospheric Deposition (TTADs) calculated**  
 1455 **from soluble Fe contained in aerosols estimated from a two-stage sequential leach (UHP water, then 25%**  
 1456 **HAc, Shelley et al., this issue). Note that numbers on top of points represent station numbers and that the**  
 1457 **colour coding refers to different region with in yellow, margin stations; in purple, the West European Basin;**  
 1458 **in blue, the Iceland Basin; in green, the Irminger Sea and in red, the Labrador Sea. The numbers on top of**  
 1459 **the plot represent TTADs averaged for each oceanic basin and their standard deviation.**



1460  
 1461

1462 Figure 7: Section plot of the Fe\* tracer in the North Atlantic Ocean with a remineralization rate ( $R_{Fe:N}$ ) of 0.05  
 1463 mmol mol<sup>-1</sup> from surface to 225 m depth. A contour line of 0 separates areas of negative Fe\* from areas  
 1464 with positive Fe\*. Positive values of Fe\* imply there is enough iron to support complete consumption of  
 1465 NO<sub>3</sub><sup>-</sup> when this water is brought to surface, and negative Fe\* values imply a deficit. See text for details.



1466  
 1467  
 1468  
 1469  
 1470  
 1471  
 1472  
 1473  
 1474  
 1475

1476

1477 Table 1: Station number, date of sampling (in the DD/MM/YYYY format), size pore used for filtration  
1478 ( $\mu\text{m}$ ), station location, mixed layer depth (m) and associated average dissolved iron (DFe)

1479 concentrations, standard deviation and number of samples during the GEOTRACES GA01 transect.

1480 Note that the asterisk next to station numbers refers to disturbed temperature and salinity profiles as

1481 opposed to uniform profiles.

Station	Date sampling	filtration $\mu\text{m}$	Latitude $^{\circ}\text{N}$	Longitude $^{\circ}\text{E}$	$Z_m$ m	DFe ( $\text{nmol L}^{-1}$ )		
	DD/MM/YYYY					average	SD	n
1	19/05/2014	0.2	40.33	-10.04	25.8	1.07	$\pm$ 0.12	1
2	21/05/2014	0.2	40.33	-9.46	22.5	1.01	$\pm$ 0.04	1
4	21/05/2014	0.2	40.33	-9.77	24.2	0.73	$\pm$ 0.03	1
11	23/05/2014	0.2	40.33	-12.22	31.3	0.20	$\pm$ 0.11	2
13	24/05/2014	0.45	41.38	-13.89	18.8	0.23	$\pm$ 0.02	1
15	28/05/2014	0.2	42.58	-15.46	34.2	0.22	$\pm$ 0.03	2
17	29/05/2014	0.2	43.78	-17.03	36.2	0.17	$\pm$ 0.01	1
19*	30/05/2014	0.45	45.05	-18.51	44.0	0.13	$\pm$ 0.05	2
21	31/05/2014	0.2	46.54	-19.67	47.4	0.23	$\pm$ 0.08	2
23*	02/06/2014	0.2	48.04	-20.85	69.5	0.21	$\pm$ 0.05	6
25	03/06/2014	0.2	49.53	-22.02	34.3	0.17	$\pm$ 0.04	2
26	04/06/2014	0.45	50.28	-22.60	43.8	0.17	$\pm$ 0.03	2
29	06/06/2014	0.45	53.02	-24.75	23.8	0.17	$\pm$ 0.02	1
32	07/06/2014	0.2	55.51	-26.71	34.8	0.59	$\pm$ 0.08	2
34	09/06/2014	0.45	57.00	-27.88	25.6	NA	$\pm$	0

36	10/06/2014	0.45	58.21	-29.72	33.0	0.12	±	0.02	1
38	10/06/2014	0.45	58.84	-31.27	34.5	0.36	±	0.16	2
							±		
40	12/06/2014	0.45	59.10	-33.83	34.3	0.39	P	0.05	1
42	12/06/2014	0.45	59.36	-36.40	29.6	0.36	±	0.05	1
44	13/06/2014	0.2	59.62	-38.95	25.8	NA	±		0
49	15/06/2014	0.45	59.77	-41.30	60.3	0.30	±	0.05	2
53*	17/06/2014	0.45	59.90	-43.00	36.4	NA	±		0
56*	17/06/2014	0.45	59.82	-42.40	30.0	0.87	±	0.06	1
60*	17/06/2014	0.45	59.80	-42.00	36.6	0.24	±	0.02	2
61*	19/06/2014	0.45	59.75	-45.11	39.8	0.79	±	0.12	1
63*	19/06/2014	0.45	59.43	-45.67	86.7	0.40	±	0.03	1
64	20/06/2014	0.45	59.07	-46.09	33.9	0.27	±	0.06	2
68*	21/06/2014	0.45	56.91	-47.42	26.3	0.22	±	0.01	1
69*	22/06/2014	0.45	55.84	-48.09	17.5	0.24	±	0.02	1
71	24/06/2014	0.45	53.69	-49.43	36.7	0.32	±	0.04	2
77*	26/06/2014	0.45	53.00	-51.10	26.1	NA	±		0
78	27/06/2014	0.45	51.99	-53.82	13.4	0.79	±	0.05	1

1482  
1483  
1484  
1485  
1486  
1487

1488 **Table 2: SAFe S, GSP and NASS-7 dissolved iron concentrations (DFe, nmol L<sup>-1</sup>) determined by the**  
 1489 **SeaFAST-pico™ and their consensus (SAFe S, GSP;**  
 1490 **<https://websites.pmc.ucsc.edu/~kbruland/GeotracesSaFe/kwbGeotracesSaFe.html> and certified (NASS-7;**  
 1491 **[https://www.nrc-cnrc.gc.ca/eng/solutions/advisory/crm/certificates/nass\\_7.html](https://www.nrc-cnrc.gc.ca/eng/solutions/advisory/crm/certificates/nass_7.html)) DFe concentrations. Note**  
 1492 **that yet no consensual value is reported for the GSP seawater.**  
 1493

Seawater used for calibration	SeaFAST-pico™ DFe values (nmol L <sup>-1</sup> )			reference or certified DFe values (nmol L <sup>-1</sup> )		
	Average	SD	n	Average	SD	
SAFe S	0.100	± 0.006	2	0.095 ±	0.008	
GSP	0.16	± 0.04	15	NA ±	NA	
NASS-7	6.7	± 1.7	12	6.3 ±	0.5	

1494  
 1495  
 1496  
 1497  
 1498  
 1499  
 1500  
 1501  
 1502  
 1503  
 1504  
 1505  
 1506  
 1507  
 1508  
 1509  
 1510

1511 Table 3: Averaged DFe:DAI (Menzel Barraqueta et al., 2018) and PFe:PAI (Gourain et al., in prep.2019)  
 1512 ratios reported per margins. Note that to avoid phytoplankton uptake, only depth below 100 m depth are  
 1513 considered.  
 1514

Margins	Stations	DFe:DAI (mol:mol)		PFe:PAI (mol:mol)		DFe:PFe (mol:mol)		n	
		#	average	SD	average	SD	average		SD
<i>Iberian Margin</i>	2 and 4		0.07	± 0.03	0.20	± 0.01	0.13	± 0.09	10
<i>East Greenland Margin</i>	56 and 53		0.21	± 0.09	0.30	± 0.01	0.12	± 0.03	6
<i>West Greenland Margin</i>	61		0.18	± 0.02	0.32	± 0.01	0.14	± 0.04	3
<i>Newfoundland Margin</i>	78		1.1	± 0.41	0.31	± 0.01	0.06	± 0.02	4

1515  
 1516